SEMARAK ILMU PUBLISHING

Journal of Advanced Research in Fluid Mechanics and Thermal Sciences

Journal homepage:
https://semarakilmu.com.my/journals/index.php/fluid_mechanics_thermal_sciences/index
ISSN: 2289-7879

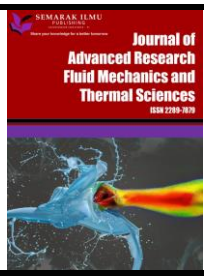

New Analytical Study of Heat Transfer Analysis of Jeffery–Hamel Nanofluid Flow Problem with Porous Medium

Saja Isam Abdulridah[1,*], Abeer Majeed Jasim[1]

[1] Department of Mathematics, College of Science, University of Basrah, Basrah, Iraq

ARTICLE INFO

Article history:
Received 5 September 2022
Received in revised form 11 January 2023
Accepted 17 January 2023
Available online 5 February 2023

Keywords:
Jeffrey Hamel; magnetohydrodynamics; nanofluid flow; nanoparticles; non-parallel plates; Perturbation Iteration Scheme; porous medium

ABSTRACT

In this study, a perturbation iteration scheme (PIS), is used to investigate the flow and heat transfer of a nanofluid through a convergent or divergent channel in a porous medium for the Jeffrey Hamel flow problem. Under the influence of the magnetic field, the nanofluid continuously flows through the channel. Modeling of the motion of different nanofluids is done with the aid of momentum and energy equations. The effect of some variables such as opening channel angle, Reynolds number ($\Re$), Darcy number (D_a), Hartmann number ($\mathcal{H}$), Prandtl number (P_r), and Eckert number ($\mathrm{E_c}$), on nanofluidic flows through non-parallel plates has been discussed. It has been observed that as velocity rises, fluid viscosity increases with a higher Reynolds number. The internal friction also decreases as the Darcy number rises because of an increase in flow and an increase in heat transfer. Additionally, when the results of the remaining variables were examined and their effects on the velocity and temperature profiles were compared with those of related studies in the literature, a satisfactory level of agreement was found. This is clear from the tables and drawings mentioned in this manuscript, and it also shows that this approach gives us a good study for examining the Jeffrey Hamel problem.

1. Introduction

Between 1915 and 1916, Jeffery and Hamel suggested a diverging and convergent channel flow. Even though this subject has been studied for a long time, little has been done. However, flow through this porous medium does have important and useful applications, such as blood flow through arteries and veins, which are tubes that carry blood to and from the heart. In contrast to arteries, veins widen as blood leaves the heart and returns to them. Both convergent and divergent behaviour is displayed here. Environmental engineering applications include channels like dams and irrigation canals, among many others, and these structures can all be seen to have similar transport phenomena. The particle composition was described using this information by Chen *et al.,* [1]. As porous media, clusters serve a purpose. The existence of tiny pore clusters is shown by this. In reservoir beds, waste removal, catalytic converters, and geothermal systems, porous medium flows

* *Corresponding author.*
E-mail address: saja.issam2@gmail.com

https://doi.org/10.37934/arfmts.103.1.105132

are used. The range of the Darcy number [2-12], governs the flow of a porous medium. Low Reynolds numbers show the validity of Farad *et al.,* Darcy's theory, and values in the range of one to ten are also low. According to Alfven *et al.,* [13], conducting flowing nanofluid produces electromotive force, which alters the velocity distribution profile. Electric forces are produced by induced current flows. As a result, magnetohydrodynamic fluid flow through porous media has discovered a variety of fascinating applications in contemporary engineering, including plasma physics, nuclear reactors, and the extraction of renewable energy, to name a few [14-19]. Other researchers have conducted studies based on this ground-breaking work. Raftari and Vajravelu [20] presented a method for calculating the flow and heat transfer through stretching walls while taking the magnetic field's influence into account. Hatami *et al.,* [21], investigation into the movement of nanofluids on a flat plate in a magnetic force field that is always present. Sheikholeslami *et al.,* [22-26] investigated heat transfer, entropy production, and nanofluid flow using a variety of flow channels. The localized heated natural convective flow was demonstrated by Hussein and Mustafa [27] using a water-copper nanofluid. In their study Prabhakar *et al.,* [28], took slip and thermal radiation into account as they looked at the stagnation point flow of an MHD nanofluid over a convective surface. Al-Mdallal [29], investigated the entropy generation analysis of a wavy sinusoidal channel containing a nanofluid made of methanol. In his paper Ganesh [30], investigated second order thermal slip and Newtonian fluid flow with entropy. Aman *et al.,* [31] studied the MHD Maxwell fluid's slip effect and heat transfer in a porous medium. Ganesh *et al.,* [32] looked into the Maragoni boundary layer flow over a stretching sheet under non-linear thermal radiative conditions. because nonlinear systems of equations are a common representation of real-world problem. Analyzing these problems requires the use of a suitable, dependable, and accurate method of solution. As a result, in the analysis of these problem, researchers have gradually adopted approximative analytical, semi-analytical, and numerical solution methods. There are several methods for finding solutions, including the Variation of Parameters Method (VPM), Differential Transform Method (DTM), Differential Transform-Pade Method (an extension solution of DTM), Collocation, Least-square, and Galerkin methods of weighted residuals, Adomian Decomposition Method (ADM), Homotopy Perturbation Method (HPM), Variational Iteration Method (VIM), and Perturbation Iteration Scheme (PIS) [33-61]. Rounding errors and limitations apply to the methods mentioned above. The PIS was chosen as the practical, accurate approach in this article because it does not rely on linearization, discretization, or small perturbation parameters. Applying this algorithm allows for the definition of new initial conditions to solve the Jeffrey Hamel flow problem. The theoretical framework of this study is to study the flow problem of the ordinary non-linear equation and its importance in addressing the problems that occur when flowing nanofluids using approximate analytical numerical methods, and one of these methods is the perturbed scheme, as in this method we take it upon ourselves to find approximate analytical solutions to the problem of the flow of Jeffrey Hamel Through diverging / converging channels and also controlling the physical parameters to obtain the best results through changing the parameters of viscosity, density, volume fraction coefficient, Reynolds number, Hartmann number, Darcy number, open angle and other parameters as changing these parameters gives us a better view of the How the flow flows through the channels, and also do not forget to review previous literature and compare them for better results [63]. Physical parameters like the Hartmann parameter, Reynold number, Darcy number, Prandtl number, and Eckert number are contained in these series and can be compensated for by constants. The effects of these parameters on the velocity and temperature profiles will be examined. An electrically conducting magnetohydrodynamic MHD nanofluid is flowed through a diverging or convergent channel with a porous medium in this study to examine the effects of heat transfer and flow while taking internal heat production into account. Moreover, using the Runge-Kutta method of fourth order (RK~4), this

study includes addressing the non-linear Jeffrey Hamel equation in nanofluids using PIS, as the solution to this equation has not been previously addressed in this way, the new analytical solutions were compared to the obtained numerical solutions. Here is a quick rundown of the paper's consistency: The governing statement problem is illustrated in Section 2 of the paper. The application of by PIS has been written in Section 3. Results and discussions are clarified in Section 4. Finally, the conclusions are introduced in Section 5.

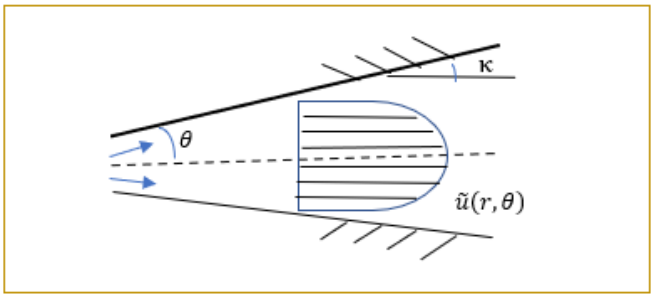

Fig. 1. Diagram of the problem [56]

2. Mathematical Formulation

The nanofluid flow that is being thought about in this situation is incompressible, two-dimensional, and electrically conducting. In order to describe the flow through the channel, cylindrical coordinates (r, θ, z) are used because intersecting planes are in the z axis. Pure radial motion is assumed because the fluid parameters do not change. The fluid is therefore moving at axis r. This is shown in Figure 1. The terminology used by Naiver Stokes to describe the viscous flow governing equation system comes from the nomenclature discussed in [22,56].

$$\frac{\rho}{r}\frac{\partial(r\tilde{u})}{\partial r}(r\tilde{u}(r,\theta)) = 0 \tag{1}$$

$$\tilde{u}\frac{\partial\tilde{u}}{\partial r} = \frac{-1}{\rho_{n.f}}\frac{\partial P}{\partial r} + \nu_{n.f}\left[\frac{\partial^2\tilde{u}}{\partial r^2} + \frac{1}{r}\frac{\partial\tilde{u}}{\partial r} + \frac{1}{r^2}\frac{\partial^2\tilde{u}}{\partial\theta^2} - \frac{\tilde{u}}{r^2}\right] - \left[\frac{\sigma_{n.f}B_o^2}{\rho_{n.f}r^2} - \frac{\mu}{K_p r^2}\right]\tilde{u}(r,\theta) \tag{2}$$

$$-\frac{1}{r\rho_{n.f}}\frac{\partial P}{\partial\theta} + \frac{2\nu_{n.f}}{r^2}\frac{\partial\tilde{u}}{\partial\theta} = 0 \tag{3}$$

$$\begin{aligned}\left(\rho C_\rho\right)_{n.f}\tilde{u}\frac{\partial T}{\partial r} = k_{n.f}\left[\frac{\partial^2 T}{\partial r^2} + \frac{1}{r}\frac{\partial T}{\partial r} + \frac{1}{r^2}\frac{\partial^2 T}{\partial\theta^2}\right] + \mu_{n.f}\left[2\left(\left(\frac{\partial\tilde{u}}{\partial r}\right)^2 + \left(\frac{\tilde{u}}{r}\right)^2\right) + \frac{1}{r^2}\left(\frac{\partial\tilde{u}}{\partial\theta}\right)^2\right] \\ +\sigma B_o^2\frac{\tilde{u}^2}{r} + Q(T - T_w)\end{aligned} \tag{4}$$

where $\tilde{u}$ is the velocity in the radial direction, P is the fluid pressure, $\rho_{n.f}$ the nanofluid viscosity coefficient density, and $K_{n.f}$ is thermal conductivity of the nanofluid, K_f and K_s are the thermal conductivity of the base fluid and the solid of fraction, respectively. The dynamic viscosity that is effective $\mu_{n.f}$ and the effective density $\rho_{n.f}$, the nanofluid calculated as follows [56]

i. $\rho_{n.f} = (1-\varphi)\rho_f + \varphi\rho_s$,

ii. $\mu_{n.f} = \frac{\mu_f}{(1-\varphi)^{2.5}}$,

iii. $\nu_{n.f} = \frac{\mu_f}{\rho_{n.f}}$,

iv. $\frac{\sigma_{n.f}}{\sigma_f} = 1 + \frac{3(\frac{\sigma_s}{\sigma_f}-1)\varphi}{(\frac{\sigma_s}{\sigma_f}+2)-(\frac{\sigma_s}{\sigma_f}-1)\varphi}$. (5)

The nanoparticle concentration is denoted by φ, $(\rho C_\rho)_{n.f}$ is the heat capacity of the nanofluid, and ρ_f and ρ_s are the densities of the base fluid and the solid fractions, respectively. If $u_\theta = 0$ for purely radial flow, the velocity parameter can from Eq. (1), by product both sides by $(\frac{r}{\rho}) \neq 0$ and then integration for (r) and put the integration constant for θ

$$\frac{\partial(r\tilde{u})}{\partial r}(r\tilde{u}) = 0, \qquad r\tilde{u}(r,\theta) = \hbar(\theta). \tag{6}$$

Also, derivative Eq. (2) and Eq. (3) with respect to (r) and (θ) respectively, gets

$$\frac{\tilde{u}(\partial^2\tilde{u})}{\partial r\,\partial\theta} + \frac{\partial\tilde{u}}{\partial r}\frac{\partial\tilde{u}}{\partial\theta} = -\frac{1}{\rho_{n.f}}\frac{\partial^2 P}{\partial r\,\partial\theta} + \nu_{n.f}\left[\frac{\partial^3\tilde{u}}{\partial r^2\,\partial\theta} + \frac{1}{r}\frac{\partial^2\tilde{u}}{\partial r\,\partial\theta} + \frac{1}{r^2}\frac{\partial^3\tilde{u}}{\partial\theta^3} - \frac{1}{r^2}\frac{\partial\tilde{u}}{\partial\theta}\right] - \left[\frac{\sigma_{n.f}B_0^2}{\rho_{n.f}r^2} - \frac{\mu}{K_p r^2}\right]\frac{\partial\tilde{u}}{\partial\theta}, \tag{7}$$

$$-\frac{1}{r\rho_{n.f}}\frac{\partial^2 P}{\partial r\,\partial\theta} + \frac{1}{r^2\rho_{n.f}}\frac{\partial P}{\partial\theta} + \frac{2\nu_{n.f}}{r^2}\frac{\partial^2\tilde{u}}{\partial r\,\partial\theta} - \frac{4\nu_{n.f}}{r^3}\frac{\partial\tilde{u}}{\partial\theta} = 0\,. \tag{8}$$

After arrangement for Eq. (7) and Eq. (8), the following equation are given as

$$\frac{\tilde{u}(\partial^2\tilde{u})}{\partial r\,\partial\theta} + \frac{\partial\tilde{u}}{\partial r}\frac{\partial\tilde{u}}{\partial\theta} = \nu_{n.f}\left[\frac{\partial^3\tilde{u}}{\partial r^2\,\partial\theta} - \frac{1}{r}\frac{\partial^2\tilde{u}}{\partial r\,\partial\theta} + \frac{1}{r^2}\frac{\partial^3\tilde{u}}{\partial\theta^3} + \frac{1}{r^2}\frac{\partial\tilde{u}}{\partial\theta}\right] - \left[\frac{\sigma_{n.f}B_0^2}{\rho_{n.f}r^2} - \frac{\mu}{K_p r^2}\right]\frac{\partial\tilde{u}}{\partial\theta}, \tag{9}$$

since

$$\hbar(\varkappa) = \frac{\hbar(\theta)}{u_c}, \qquad \tilde{u}(r,\theta) = \frac{u_c}{r}\hbar(\varkappa), \qquad \varkappa = \frac{\theta}{\kappa}, \tag{10}$$

also

$$r^2\frac{T}{T_w} = \Theta(\varkappa), \qquad T(r,\theta) = \frac{T_w}{r^2}\Theta(\varkappa). \tag{11}$$

Now, find the partial derivative of Eq. (9) and Eq. (4), by using Eq. (10) and Eq. (11)

$$\frac{\partial\tilde{u}}{\partial\theta} = \frac{u_c}{\kappa r}\left(\frac{d\hbar(\varkappa)}{d\varkappa}\right) \qquad \frac{\partial^2\tilde{u}}{\partial\theta^2} = \frac{u_c}{\kappa^2 r}\left(\frac{d^2\hbar(\varkappa)}{d\varkappa^2}\right) \qquad \frac{\partial^3\tilde{u}}{\partial\theta^3} = \frac{u_c}{\kappa^3 r}\left(\frac{d^3\hbar(\varkappa)}{d\varkappa^3}\right)$$

$$\frac{\partial^2\tilde{u}}{\partial r\,\partial\theta} = \frac{-u_c}{\kappa r^2}\left(\frac{d\hbar(\varkappa)}{d\varkappa}\right) \qquad \frac{\partial\tilde{u}}{\partial r} = \frac{-u_c}{r^2}\hbar(\varkappa) \qquad \frac{\partial^2\tilde{u}}{\partial r^2} = \frac{2u_c}{r^3}\hbar(\varkappa)$$

$$\frac{\partial^3\tilde{u}}{\partial r^2\,\partial\theta} = \frac{2u_c}{\kappa r^3}\left(\frac{d\hbar(\varkappa)}{d\varkappa}\right) \qquad \frac{\partial T}{\partial r} = \frac{-2T_w}{r^3}\Theta(\varkappa) \qquad \frac{\partial T}{\partial\theta} = \frac{T_w}{\kappa r^2}\left(\frac{d\Theta(\varkappa)}{d\varkappa}\right)$$

$$\frac{\partial^2 T}{\partial\theta^2} = \frac{T_w}{\kappa^2 r^2}\left(\frac{d^2\Theta(\varkappa)}{d\varkappa^2}\right) \qquad \frac{\partial^2 T}{\partial r^2} = \frac{6T_w}{\kappa r^4}\left(\frac{d\Theta(\varkappa)}{d\varkappa}\right). \tag{12}$$

Substituting Eq. (10) into Eq. (9) and Eq. (4) become

$$\frac{u_c}{r}\hbar(\varkappa)\frac{-u_c}{\kappa r^2}\frac{d\hbar(\varkappa)}{d\varkappa}+\frac{-u_c}{r^2}\hbar(\varkappa)\frac{u_c}{\kappa r}\frac{d\hbar(\varkappa)}{d\varkappa}=\nu_{n.f}\left[\frac{2u_c}{\kappa r^3}\frac{d\hbar(\varkappa)}{d\varkappa}-\frac{1}{r}\left(\frac{-u_c}{\kappa r^2}\frac{d\hbar(\varkappa)}{d\varkappa}\right)+\frac{1}{r^2}\frac{u_c}{\kappa^3 r}\frac{d^3\hbar(\varkappa)}{d\varkappa^3}+\frac{1}{r^2}\frac{u_c}{\kappa r}\frac{d\hbar(\varkappa)}{d\varkappa}\right]-\left[\frac{\sigma_{n.f}B_0^2}{\rho_{n.f}r^2}-\frac{\mu}{K_p r^2}\right]\frac{u_c}{\kappa r}\left(\frac{d\hbar(\varkappa)}{d\varkappa}\right), \tag{13}$$

Simplify Eq. (13) more to get

$$-\frac{2{u_c}^2}{\kappa r^3}\hbar(\varkappa)\frac{d\hbar(\varkappa)}{d\varkappa}=\nu_{n.f}\left[\frac{4u_c}{\kappa r^3}\frac{d\hbar(\varkappa)}{d\varkappa}+\frac{u_c}{\kappa^3 r^3}\frac{d^3\hbar(\varkappa)}{d\varkappa^3}\right]-\left[\frac{\sigma_{n.f}B_0^2}{\rho_{n.f}}-\frac{\mu}{K_p}\right]\frac{u_c}{\kappa r^3}\left(\frac{d\hbar(\varkappa)}{d\varkappa}\right). \tag{14}$$

Product both sides by $\left(\frac{\kappa^3 r^3}{u_c \nu_{n.f}}\neq 0\right)$, and by using Eq. (5) to get after simplify

$$\frac{d^3\hbar(\varkappa)}{d\varkappa^3}-\kappa\left[\left(B^*\mathcal{H}(1-\varphi)^{1.25}\right)\frac{1}{D_a}-4\right]\frac{d\hbar(\varkappa)}{d\varkappa}+2A^*\Re\kappa(1-\varphi)^{2.5}\hbar(\varkappa)\frac{d\hbar(\varkappa)}{d\varkappa}. \tag{15}$$

Also, from Eq. (4) and by substituting Eq. (12), yield

$$\left(\rho C_\rho\right)_{n.f}\left(\frac{u_c}{r}\hbar(\varkappa).\frac{-2T_w}{r^3}\Theta(\varkappa)\right)=k_{n.f}\left[\frac{6T_w}{\kappa r^4}\left(\frac{d\theta(\varkappa)}{d\varkappa}\right)+\frac{-2T_w}{r^3}\Theta(\varkappa)+\frac{T_w}{\kappa^2 r^2}\frac{d^2\Theta(\varkappa)}{d\varkappa^2}\right]+\mu_{n.f}\left[2\left(\frac{u_c^2}{r^4}\left(\hbar(\varkappa)\right)^2+\frac{u_c^2}{r^2}\left(\hbar(\varkappa)\right)^2\right)+\frac{u_c^2}{\kappa^2 r^4}\left(\frac{d\hbar(\varkappa)}{d\varkappa}\right)^2\right], \tag{16}$$

by using Eq. (5), the Eq. (16) become as

$$\left[\frac{d^2\Theta(\varkappa)}{d\varkappa^2}+4\kappa^2\Theta(\varkappa)+\frac{A^*}{B^*}2P_r\kappa^2\hbar(\varkappa)\Theta(\varkappa)+\frac{P_r E_c}{\Re B^*(1-\varphi)^{2.5}}\left(4\kappa^2\left(\hbar(\varkappa)\right)^2+\left(\frac{d\hbar(\varkappa)}{d\varkappa}\right)^2\right)\right]+\frac{P_r E_c\mathcal{H}}{B^*}\left(\hbar(\varkappa)\right)^2+\xi\Theta(\varkappa)=0, \tag{17}$$

with boundary conditions as

$$\hbar(0)=1,\ \ \frac{d\hbar(0)}{d\varkappa}=0,\ \ \hbar(1)=0,\ \ \Theta(1)=1,\ \ \frac{d\Theta(0)}{d\varkappa}=0, \tag{18}$$

where

$$\Re=\frac{u_c}{V_f}=\frac{U_{max}r}{V_f}\times\begin{pmatrix}\text{divergent}-\text{channel}:\kappa>0,u_c>0\\ \text{convergent}-\text{channel}:\kappa<0,u_c<0\end{pmatrix},\ P_r=\frac{\mu_f(C_\rho)_f}{K_f},\ E_c=\frac{u_c^2}{T_w(C_\rho)_f} \tag{19}$$

$$\mathcal{H}=\sqrt{\frac{\sigma_f B_o^2}{\rho_f \nu_f}},\ D_a=\frac{\mu u}{K_\rho},\ \xi=\frac{QA\left(\rho C_\rho\right)_{n.f}}{K_{n.f}(T-T_w)},\ A^*=(1-\varphi)+\frac{\rho_s}{\rho_f}\varphi,\ B^*=1+\frac{3\left(\frac{\sigma_s}{\sigma_f}-1\right)\varphi}{\left(\frac{\sigma_s}{\sigma_f}+2\right)-\left(\frac{\sigma_s}{\sigma_f}-1\right)\varphi}. \tag{20}$$

Physically, these boundary constraints imply that maximum velocity values are seen at the centreline ($\varkappa=0$), and consider the velocity profile to be completely developed, therefore the rate of velocity is zero at ($\varkappa=0$). The no-slip requirement is also used in fluid dynamics. The equation for fluid states that the fluid will have zero pressure at a solid barrier related to the boundary velocity at all fluid–solid interfaces, the fluid velocity it can observe that the solid boundary border is equal to the solid boundaries. Numerous processes, including large-scale chemical reactions involving

catalyst, filter, and adsorbent, as well as the modelling of physiological processes, involve flow through porous media. These processes include geophysical flow, the recovery of oil, gas, and minerals from the earth, the transport and sequestration of contaminants in the subsurface, and many others. Due to the rapidly expanding use of magnetohydrodynamic (MHD) flows of viscous fluids in many areas of technology and engineering, such as MHD power generation, MHD flow meters, and MHD pumps, numerous theoretical investigations involving these flows have been conducted in recent decades. The behaviour of the viscous MHD flow under various conditions has been explained by several mathematical models [64,65]. To account for the effects of an external magnetic field on conducting fluid, the original Jeffery-Hamel problem was expanded. For fluids with a moderate Prandtl number and moderate velocities, small wall-to-fluid temperature differences, low wall heat fluxes, and flowing through parallel walls, the effect of viscous dissipation on heat transfer is particularly important. Then in general flow through porous media has a myriad of applications ranging from geophysical flow and recovery of oil, gas, minerals and other nanofluids to large-scale chemical processes involving catalyst and filtrate as well as modelling of physiological processes. Many theoretical investigations dealing with MHD flows have been conducted. of viscous fluids during the past decades due to its rapidly increasing applications in many areas of technology and engineering such as MHD power generation, MHD flow meters, MHD pumps. Undoubtedly the viscous dissipation yields an appreciable rise in fluid temperature. This is because of the conversion of kinetic motion of fluid to thermal energy and characteristics of source term in the fluid flow. Especially such situation is prominent for fluid flow with heat transfer in microchannels where length-to-diameter ration is very large [66-68].

3. Implementation Perturbation Iteration Scheme for Solving heat transfer on Jeffery-Hamel Nanofluid Flow

We carried out this study to obtain an approximate analytical solution to the Jeffrey Hamel equation and to examine the behaviour of the physical parameters when taking different values of them and the behaviour of the nanofluid flow through the divergent/convergent channels. This study dealt with the flow of nanofluids for different materials such as (copper, silver, titanium and aluminium) as the use of this method was used for the first time on this type of equation and proved its effectiveness when obtaining excellent results and compared with other results in the previous literature and its efficiency is clear and accurate. The application of the PIS (1,1) [62], to nonlinear differential equations using the stages of its method in order to obtain approximate analytical solutions. The following is an illustration of the auxiliary perturbation parameter δ can be given as:

$$\mathrm{Q}_1\left(\hbar(\varkappa),\frac{\partial\hbar(\varkappa)}{\partial\varkappa},\frac{\partial^3\hbar(\varkappa)}{\partial\varkappa^3},\delta\right)=\frac{\mathrm{d}^3\hbar(\varkappa)}{\mathrm{d}\varkappa^3}-\delta\kappa\left[(B^*\mathcal{H}(1-\varphi)^{1.25})\frac{1}{D_a}-4\right]\frac{\mathrm{d}\hbar(\varkappa)}{\mathrm{d}\varkappa}$$
$$+2\delta A^*\Re\kappa(1-\varphi)^{2.5}\hbar(\varkappa)\frac{\mathrm{d}\hbar(\varkappa)}{\mathrm{d}\varkappa}, \quad (21)$$

$$\mathrm{Q}_2(\hbar(\varkappa),\frac{\partial\hbar(\varkappa)}{\partial\varkappa},\Theta(\varkappa),\frac{\partial^2\Theta(\varkappa)}{\partial\varkappa^2},\delta)=\frac{\mathrm{d}^2\Theta(\varkappa)}{\mathrm{d}\varkappa^2}+\delta\,4\kappa^2\Theta(\varkappa)+\delta\frac{A^*}{B^*}2\mathrm{P_r}\kappa^2\hbar(\varkappa)\Theta(\varkappa)+$$
$$\frac{\mathrm{P_rE_c}}{\Re B^*(1-\varphi)^{2.5}}\delta(4\kappa^2\left(\hbar(\varkappa)\right)^2+\left(\frac{\mathrm{d}\hbar(\varkappa)}{\mathrm{d}\varkappa}\right)^2))+\frac{\mathrm{P_rE_c}\mathcal{H}}{B^*}\delta\left(\hbar(\varkappa)\right)^2+\delta\xi\Theta(\varkappa)=0. \quad (22)$$

where $\hbar$ is an unknown function and special dependent variable. Q is a function of $\hbar$ and its derivatives. The auxiliary perturbation parameter δ was added to Eq. (21), as indicated in the equation above. The following are perturbation expansions that only include one correction term

$$\hbar_{n+1} = \hbar_n + \delta(\hbar_c)_n, \tag{23}$$

$$\Theta_{n+1} = \Theta_n + \delta(\Theta_c)_n \ , \tag{24}$$

where $\hbar_C$ and Θ_c is the correction term in the perturbation expansion, substituting Eq. (22) and Eq. (24) in Eq. (21) and Eq. (22), respectively and expanding in Taylor series with first -order derivative with term of ($\delta = 0$) to get

$$\begin{aligned} &Q_1((\hbar(\varkappa))_n, (\tfrac{d\hbar(\varkappa)}{d\varkappa})_n, (\tfrac{d^3\hbar(\varkappa)}{d\varkappa^3})_n, 0) + \delta[Q_{1\hbar_n}((\hbar(\varkappa))_c)_n + \\ &\qquad Q_{1\left(\frac{d\hbar(\varkappa)}{d\varkappa}\right)_n}((\tfrac{d\hbar(\varkappa)}{d\varkappa})_c)_n + Q_{1\left(\frac{d^3\hbar(\varkappa)}{d\varkappa^3}\right)_n}((\tfrac{d^3\hbar(\varkappa)}{d\varkappa^3})_c)_n + Q_{1\delta}] = 0, \end{aligned} \tag{25}$$

$$\begin{aligned} &Q_2((\hbar(\varkappa))_n, (\tfrac{d\hbar(\varkappa)}{d\varkappa})_n, (\tfrac{d^2\Theta(\varkappa)}{d\varkappa^2})_n, 0) + \delta[Q_{2(\hbar(\varkappa))_n}((\hbar(\varkappa))_c)_n + \\ &\qquad Q_{2(\frac{d\hbar(\varkappa)}{d\varkappa})_n}((\tfrac{d\hbar(\varkappa)}{d\varkappa})_c)_n + Q_{2\left(\frac{\partial^2\Theta(\varkappa)}{\partial\varkappa^2}\right)_n}((\tfrac{\partial^2\Theta(\varkappa)}{\partial\varkappa^2})_c)_n + Q_{2\delta}] = 0, \end{aligned} \tag{26}$$

from Eq. (21) and Eq. (22), the following derivatives

$$\begin{aligned} Q_{1\delta} &= \kappa[(B^*\mathcal{H}(1-\varphi)^{1.25})\tfrac{1}{D_a} - 4]\left(\tfrac{d\hbar(\varkappa)}{d\varkappa}\right)_n + 2A^*\Re\kappa(1-\varphi)^{2.5}\left(\hbar(\varkappa)\right)_n(\tfrac{d\hbar(\varkappa)}{d\varkappa})_n, \\ Q_{1(\frac{d\hbar(\varkappa)}{d\varkappa})_n} &= \delta\kappa[(B^*\mathcal{H}(1-\varphi)^{1.25})\tfrac{1}{D_a} - 4] + 2\delta A^*\Re\kappa(1-\varphi)^{2.5}(\hbar(\varkappa))_n \\ Q_{1(\hbar(\varkappa))_n} &= 2\delta A^*\Re\kappa(1-\varphi)^{2.5}(\tfrac{d\hbar(\varkappa)}{d\varkappa})_n \\ Q_{1(\frac{d^3\hbar(\varkappa)}{d\varkappa^3})_n} &= 1, \end{aligned} \tag{27}$$

$$\begin{aligned} Q_{2\delta} &= 4\kappa^2\left(\Theta(\varkappa)\right)_n + \tfrac{A^*}{B^*}2P_r\kappa^2\left(\hbar(\varkappa)\right)_n\left(\Theta(\varkappa)\right)_n + \tfrac{P_rE_c}{\Re B^*(1-\varphi)^{2.5}}(4\kappa^2\left(\left(\hbar(\varkappa)\right)_n\right)^2 + \\ &\qquad (\tfrac{d(\hbar(\varkappa))_n}{d\varkappa})^2))) + \tfrac{P_rE_c\mathcal{H}}{B^*}((\hbar(\varkappa))_n)^2 + \xi(\Theta(\varkappa))_n, \\ Q_{2(\hbar(\varkappa))_n} &= \delta\tfrac{A^*}{B^*}2P_r\kappa^2\Theta(\varkappa) + \tfrac{P_rE_c}{\Re B^*(1-\varphi)^{2.5}}\delta(8\kappa^2(\hbar(\varkappa))_n) + \tfrac{P_rE_c\mathcal{H}}{B^*}2\delta(\hbar(\varkappa))_n, \\ Q_{2(\Theta(\varkappa))_n} &= \delta\,4\kappa^2 + \delta\tfrac{A^*}{B^*}2P_r\kappa^2\hbar(\varkappa) + \delta\xi \\ Q_{2(\frac{d\hbar(\varkappa)}{d\varkappa})_n} &= \tfrac{P_rE_c}{\Re B^*(1-\varphi)^{2.5}}\delta((\tfrac{d(\hbar(\varkappa))_n}{d\varkappa})^2)\ , \\ Q_{2(\frac{d^2\Theta(\varkappa)}{d\varkappa^2})_n} &= 1, \end{aligned} \tag{28}$$

Note that all derivatives in Eq. (27) and Eq. (28), are calculated at $\delta = 0$, the solution in Eq. (16) and Eq. (17) is an ordinary differential equation (ODE). The boundary condition and initial condition are used to solve this ordinary differential equation, yielding $(\hbar_c)_n(\varkappa)$ and $(\Theta_c)_n(\varkappa)$. In Eq. (21) and Eq. (22), the value of $(\hbar_c)_n(\varkappa)$ and $(\Theta_c)_n(\varkappa)$ is replaced to obtain on $(\hbar_c)_{n+1}(\varkappa)$ and $(\Theta_c)_{n+1}(\varkappa)$ respectively. Which it is the approximate analytical answer, in the form of a power series, that is required. The following non-linear ordinary differential equations are obtained by computing all derivatives at ($\delta = 0$) and inserting the results into Eq. (25) and Eq. (26)

$$((\frac{\mathrm{d}^3\hbar(\varkappa)}{\mathrm{d}\varkappa^3})_{\mathrm{c}})_{\mathrm{n}} = -\frac{1}{\delta}\frac{\mathrm{d}^3(\hbar(\varkappa))_n}{\mathrm{d}\varkappa^3} + \kappa\left[(B^*\mathcal{H}(1-\varphi)^{1.25})\frac{1}{D_a} - 4\right]\frac{\mathrm{d}(\hbar(\varkappa))_n}{\mathrm{d}\varkappa} - 2A^*\Re\kappa$$
$$(1-\varphi)^{2.5}(\hbar(\varkappa))_n\frac{\mathrm{d}(\hbar(\varkappa))_n}{\mathrm{d}\varkappa}. \tag{29}$$

$$((\frac{\mathrm{d}^2\Theta(\varkappa)}{\mathrm{d}\varkappa^2})_{\mathrm{c}})_{\mathrm{n}} = -\frac{1}{\delta}\frac{\mathrm{d}^2(\Theta(\varkappa))_n}{\mathrm{d}\varkappa^2} - 4\kappa^2(\Theta(\varkappa))_n - \frac{A^*}{B^*}2\mathrm{P_r}\kappa^2(\hbar(\varkappa))_n(\Theta(\varkappa))_n - \frac{\mathrm{P_rE_c}}{\Re B^*(1-\varphi)^{2.5}}$$
$$(4\kappa^2((\hbar(\varkappa))_n)^2 + (\frac{\mathrm{d}(\hbar(\varkappa))_n}{\mathrm{d}\varkappa})^2)) - \frac{\mathrm{P_rE_c}\mathcal{H}}{B^*}((\hbar(\varkappa))_n)^2 - \xi(\Theta(\varkappa))_n, \tag{30}$$

assume that the initial condition

$$\hbar_{\mathrm{o}}(\varkappa) = \tau_{\mathrm{o}} + \tau_1\varkappa + \frac{\tau_2}{2}\varkappa^2, \tag{31}$$

$$\Theta_{\mathrm{o}}(\varkappa) = \ell_{\mathrm{o}} + \ell_1\varkappa, \tag{32}$$

where

$$\hbar(0) = \tau_{\mathrm{o}}, \qquad \frac{\mathrm{d}\hbar(0)}{\mathrm{d}\varkappa} = \tau_1, \qquad \frac{\mathrm{d}^2\hbar(\varkappa)}{\mathrm{d}\varkappa^2} = \tau_2,$$
$$\Theta(0) = \ell_{\mathrm{o}}, \qquad \frac{\mathrm{d}\Theta(\varkappa)}{\mathrm{d}\varkappa} = \ell_1. \tag{33}$$

From boundary conditions of Eq. (18)

$$\hbar_{\mathrm{o}} = 1 + \frac{\tau_2}{2}\varkappa^2, \tag{34}$$

$$\Theta_{\mathrm{o}} = \ell_{\mathrm{o}}, \tag{35}$$

The prerequisite condition for solving the problem using τ_2 and ℓ_{o} is unknown. The analytical approximate solutions of Eq. (15) and Eq. (18), at ($\varkappa = 1$) may be used to derive the values of τ_2 and ℓ_{o}.The analytical approximate solutions to the following equations are obtained by creating the iteration scheme

$$\hbar_{\mathbf{1}} = 1 + \frac{\tau_2}{2}\varkappa^2 - \left[\left(\frac{1}{24}B^*\mathcal{H}(1-\varphi)^{1.25}D_a - 4\right)\tau_2 - \frac{1}{12}\kappa\Re A^*(1-\varphi)^{2.5}\tau_2\right]\varkappa^4 - \frac{1}{120}$$
$$\kappa\Re A^*(1-\varphi)^{2.5}\tau_2^2\varkappa^6. \tag{36}$$

$$\boldsymbol{\Theta_1} = \ell_{\mathrm{o}} - \frac{1}{2}(4\kappa^2\ell_{\mathrm{o}} + \frac{2A^*P_r\kappa^2\ell_{\mathrm{o}}}{B^*} + \frac{4P_rE_c\kappa^2}{\Re B^*(1-\varphi)^{2.5}} + \frac{P_rE_c\mathcal{H}}{B^*} + \xi\ell_{\mathrm{o}})\varkappa^4 - \frac{1}{12}(\frac{A^*P_r\kappa^2\tau_2\ell_{\mathrm{o}}}{B^*}$$
$$+ \frac{P_rE_c(4\kappa^2\tau_2+\tau_2^2)}{\Re B^*(1-\varphi)^{2.5}} + \frac{P_rE_c\mathcal{H}\tau_2}{B^*})\varkappa^4 - (\frac{1}{30}\frac{P_rE_c\kappa^2\tau_2^2}{\Re B^*(1-\varphi)^{2.5}}\frac{1}{120}\frac{P_rE_c\mathcal{H}\tau_2^2}{B^*})\varkappa^6 \tag{37}$$

$$\hbar_{\mathbf{2}} = 1 + \frac{\tau_2}{2}\varkappa^2 - [\frac{1}{6}\kappa(B^*\mathcal{H}(1-\varphi)^{1.25}D_a - 4)\tau_2 - \frac{1}{3}\kappa\Re A^*(1-\varphi)^{2.5}\tau_2 - \frac{3.33333333\times10^{-11}}{4}$$
$$\kappa\Re A^*(1-\varphi)^{2.5}]\varkappa^4 - [\frac{1}{120}\kappa\Re A^*(1-\varphi)^{2.5}\tau_2^2 - \frac{1}{720}\kappa^2(B^*\mathcal{H}(1-\varphi)^{1.25}D_a - 4)^2\tau_2 -$$
$$\frac{2}{360}\kappa^2\Re A^*(1-\varphi)^{2.5}(B^*\mathcal{H}(1-\varphi)^{1.25}D_a - 4)\tau_2 - \frac{1}{180}\kappa^2\Re A^*(1-\varphi)^{2.5}\tau_2^2]\varkappa^6 -$$
$$[\frac{0.001190476191}{8}\kappa^2\Re A^*(1-\varphi)^{2.5}(B^*\mathcal{H}(1-\varphi)^{1.25}D_a - 4)\tau_2^2 - \frac{0.002380952382}{8}\kappa^2\Re^2A^{*2}$$
$$(1-\varphi)^5\tau_2^2 + \frac{0.002380952382}{8}\kappa^2\Re A^*(1-\varphi)^{2.5}(B^*\mathcal{H}(1-\varphi)^{1.25}D_a - 4)\tau_2^2 - \frac{1}{24}\kappa^2\Re^2A^{*2}$$

$$(1-\varphi)^5\tau_2^2+\frac{0.04761904764}{192}\kappa^2\Re A^*(1-\varphi)^{2.5}\,(B^*\mathcal{H}(1-\varphi)^{1.25}D_a-4)\tau_2^2-\frac{0.04761904764}{96}$$
$$\kappa^2\Re^2A^{*2}(1-\varphi)^5\tau_2^2]\varkappa^8-[(\frac{1}{10800}\kappa^2\Re^2A^{*2}(1-\varphi)^5\tau_2^3+\frac{1}{360}\kappa\Re A^*(1-\varphi)^{2.5}\,\tau_2)$$
$$(\frac{1}{24}\kappa(B^*\mathcal{H}(1-\varphi)^{1.25}D_a-4)\tau_2-\frac{1}{12}\kappa\Re A^*(1-\varphi)^{2.5}\tau_2)(\frac{1}{6}\kappa(B^*\mathcal{H}(1-\varphi)^{1.25}D_a-4)\tau_2$$
$$-\frac{1}{3}\kappa\Re A^*(1-\varphi)^{2.5}\,\tau_2))]\varkappa^{10}-\frac{1}{12}[\frac{1}{1100}(\kappa^2\Re^2A^{*2}(1-\varphi)^5(\frac{1}{24}\kappa(B^*\mathcal{H}(1-\varphi)^{1.25}D_a-4)$$
$$\tau_2^3-\frac{1}{12}\kappa\Re A^*(1-\varphi)^{2.5}\tau_2^2)-\frac{1}{6600}\kappa^2\Re^2A^{*2}(1-\varphi)^5\tau_2^3(\frac{1}{6}\kappa(B^*\mathcal{H}(1-\varphi)^{1.25}D_a-4)$$
$$-\frac{1}{3}\kappa\Re A^*(1-\varphi)^{2.5}\,\tau_2)]\varkappa^{12}-3.815628816\times10^{-7}\kappa^3\Re^3A^{*3}(1-\varphi)^{7.5}\tau_2^4\varkappa^{14}. \qquad (38)$$

$$\mathbf{\Theta_2}=\ell_o-\left(4\kappa^2\ell_o+\frac{2\kappa^2A^*P_r\ell_o}{B^*}+\frac{4\kappa^2P_rE_c}{\Re B^*(1-\varphi)^{2.5}}+\frac{P_rE_c\mathcal{H}}{B^*}+\xi\ell_o\right)\varkappa^2-\frac{1}{3}(\frac{\kappa^2A^*P_r\tau_2\ell_o}{B^*}-\frac{P_rE_c(4\kappa^2\tau_2+\tau_2^2)}{\Re B^*(1-\varphi)^{2.5}}$$
$$-\frac{P_rE_c\mathcal{H}\tau_2}{B^*})\varkappa^3+[-\frac{1}{12}\left(\frac{\kappa^2A^*P_r\tau_2\ell_o}{B^*}+\frac{P_rE_c(4\kappa^2\tau_2+\tau_2^2)}{\Re B^*(1-\varphi)^{2.5}}+\frac{P_rE_c\mathcal{H}\tau_2}{B^*}\right)-\frac{1}{4}(\frac{4}{3}\kappa^2(-2\kappa^2\ell_o$$
$$-\frac{\kappa^2A^*P_r\ell_o}{B^*}-\frac{2\kappa^2P_rE_c}{\Re B^*(1-\varphi)^{2.5}}-\frac{P_rE_c\mathcal{H}}{B^*}-\frac{1}{2}\xi\ell_o)+\frac{1}{B^*}(\frac{2}{3}\kappa^2P_r(-2\kappa^2\ell_o-\frac{\gamma^2A^*P_r\tau_2\ell_o}{B^*}-\frac{2\kappa^2P_rE_c}{\Re B^*(1-\varphi)^{2.5}}$$
$$-\frac{1}{2}\frac{P_rE_c\mathcal{H}}{B^*}-\frac{1}{2}\xi\ell_o))+\frac{1}{3}(\frac{\kappa^2A^*P_r\tau_2\ell_o}{B^*}+\frac{P_rE_c(4\kappa^2\tau_2+\tau_2^2)}{\Re B^*(1-\varphi)^{2.5}}+\frac{P_rE_c\mathcal{H}\tau_2}{B^*}+\xi)(-2\kappa^2\ell_o$$
$$-\frac{\kappa^2A^*P_r\ell_o}{B^*}-\frac{2\kappa^2P_rE_c}{\Re B^*(1-\varphi)^{2.5}}-\frac{P_rE_c\mathcal{H}}{B^*}-\frac{1}{2}\xi\ell_o)]\varkappa^4-\frac{1}{5}[-\frac{\kappa^2P_rE_c\tau_2^2}{\Re B^*(1-\varphi)^{2.5}}-\frac{1}{4}\frac{P_rE_c\mathcal{H}\tau_2^2}{B^*}]\varkappa^5$$
$$+[(-\frac{1}{6}(\frac{1}{5}\frac{\kappa^2P_rE_c\tau_2^2}{\Re B^*(1-\varphi)^{2.5}}+\frac{1}{20}\frac{P_rE_c\mathcal{H}}{B^*}))-\frac{1}{6}(\frac{4}{60}\kappa^2(-\frac{\kappa^2A^*P_r\tau_2\ell_o}{B^*}-\frac{P_rE_c(4\kappa^2\tau_2+\tau_2^2)}{\Re B^*(1-\varphi)^{2.5}}-\frac{P_rE_c\mathcal{H}\tau_2}{B^*})$$
$$+\frac{1}{B^*}(\frac{2}{60}\kappa^2A^*P_r(-\frac{\kappa^2A^*P_r\tau_2\ell_o}{B^*}-\frac{P_rE_c(4\kappa^2\tau_2+\tau_2^2)}{\Re B^*(1-\varphi)^{2.5}}-\frac{P_rE_c\mathcal{H}\tau_2}{B^*}))+\frac{1}{B^*}(\frac{1}{5}\kappa^2A^*P_r\tau_2(-2\kappa^2\ell_o$$
$$-\frac{\kappa^2A^*P_r\ell_o}{B^*}-\frac{2\kappa^2A^*P_rE_c}{\Re B^*(1-\varphi)^{2.5}}-\frac{1}{2}\frac{P_rE_c\mathcal{H}}{B^*}-\frac{1}{2}\xi\ell_o))+\frac{1}{B^*}(\frac{2}{5}\kappa^2A^*P_r(\frac{1}{24}\kappa((B^*\mathcal{H}(1-\varphi)^{1.25}D_a4)\tau_2-$$
$$\frac{1}{12}\kappa\Re A^*(1-\varphi)^{2.5}\,\tau_2)\ell_o)+\frac{1}{\Re B^*(1-\varphi)^{2.5}}(\frac{1}{5}P_rE_c(4\kappa^2(\frac{1}{12}(B^*\mathcal{H}(1-\varphi)^{1.25}D_a-4)\tau_2-\frac{1}{6}$$
$$\Re A^*(1-\varphi)^{2.5}\,\tau_2+2\tau_2(\frac{1}{6}(B^*\mathcal{H}(1-\varphi)^{1.25}D_a-4)\tau_2-\frac{1}{3}\kappa\Re A^*(1-\varphi)^{2.5}\,\tau_2)))$$
$$\frac{1}{B^*}\left(\frac{1}{5}P_rE_c\mathcal{H}\left(\frac{1}{12}\kappa(B^*\mathcal{H}(1-\varphi)^{1.25}D_a-4)\tau_2-\frac{1}{6}\kappa\Re A^*(1-\varphi)^{2.5}\,\tau_2+\frac{1}{4}\tau_2^2\right)\right)+$$
$$\frac{1}{60}\xi(-\frac{\kappa^2A^*P_r\tau_2\ell_o}{B^*}-\frac{P_rE_c(4\kappa^2\tau_2+\tau_2^2)}{\Re B^*(1-\varphi)^{2.5}}-\frac{P_rE_c\mathcal{H}\tau_2}{B^*}))]\varkappa^6-\frac{1}{8}(0.5714285716\kappa^2(-\frac{1}{30}\frac{\kappa^2P_rE_c\tau_2^2}{\Re B^*(1-\varphi)^{2.5}}-$$
$$\frac{1}{120}\frac{P_rE_c\mathcal{H}\tau_2^2}{B^*})+\frac{1}{B^*}\left(0.2857142858\,\kappa^2A^*P_r\left(-\frac{1}{30}\frac{\kappa^2P_rE_c\tau_2^2}{\Re B^*(1-\varphi)^{2.5}}-\frac{1}{120}\frac{P_rE_c\mathcal{H}\tau_2^2}{B^*}\right)\right)+\frac{1}{B^*}(\frac{0.1428571429}{12}$$
$$\kappa^2A^*P_r\tau_2(-\frac{\kappa^2A^*P_r\tau_2\ell_o}{B^*}-\frac{P_rE_c(4\kappa^2\tau_2+\tau_2^2)}{\Re B^*(1-\varphi)^{2.5}}-\frac{P_rE_c\mathcal{H}\tau_2}{B^*}))+\frac{1}{B^*}(0.2857142858\,\kappa^2A^*P_r(\frac{19}{600}\kappa$$
$$(B^*\mathcal{H}(1-\varphi)^{1.25}D_a-4)\tau_2-\frac{1}{12}\kappa\Re A^*(1-\varphi)^{2.5}\,\tau_2)(-2\kappa^2\ell_o-\frac{\kappa^2A^*P_r\ell_o}{B^*}-\frac{2\kappa^2A^*P_rE_c}{\Re B^*(1-\varphi)^{2.5}}-$$
$$\frac{1}{2}\frac{P_rE_c\mathcal{H}}{B^*}-\frac{1}{2}\xi\ell_o))-0.002380952382\,\frac{\kappa^3A^{*2}P_r\Re(1-\varphi)^{2.5}\,\tau_2^2\ell_o}{B^*}+\frac{1}{\Re B^*(1-\varphi)^{2.5}}$$
$$(0.1428571429\,P_rE_c4\kappa^2(-\frac{1}{60}\kappa\Re A^*(1-\varphi)^{2.5}\,\tau_2^2+\tau_2(\frac{1}{24}\kappa(B^*\mathcal{H}(1-\varphi)^{1.25}D_a-4)\tau_2-$$
$$\frac{1}{12}\kappa\Re A^*(1-\varphi)^{2.5}\tau_2))\;-\frac{1}{10}\kappa\Re A^*(1-\varphi)^{2.5}\tau_2^3+(\frac{1}{6}\kappa(B^*\mathcal{H}(1-\varphi)^{1.25}D_a-4)\tau_2-$$
$$\frac{1}{3}\kappa\Re A^*(1-\varphi)^{2.5}\tau_2)^2))+\frac{1}{B^*}\,(0.1428571429\,P_rE_c\mathcal{H}(-\frac{1}{60}\kappa\Re A^*(1-\varphi)^{2.5}\tau_2^2+\tau_2$$
$$(\frac{1}{6}\kappa(B^*\mathcal{H}(1-\varphi)^{1.25}D_a-4)\tau_2-\frac{1}{12}\kappa\Re A^*(1-\varphi)^{2.5}\tau_2)))+0.1428571429\,\xi$$
$$(-\frac{1}{30}\frac{\kappa^2P_rE_c\tau_2^2}{\Re B^*(1-\varphi)^{2.5}}-\frac{1}{120}\frac{P_rE_c\mathcal{H}\tau_2^2}{B^*})]\varkappa^8-\frac{1}{10}(\frac{1}{B^*}(\frac{1}{9}\kappa^2A^*P_r\tau_2(-\frac{1}{30}\frac{\kappa^2P_rE_c\tau_2^2}{\Re B^*(1-\varphi)^{2.5}}-\frac{1}{120}\frac{P_rE_c\mathcal{H}\tau_2^2}{B^*}))+$$
$$\frac{1}{B^*}(\frac{2}{9}\kappa^2A^*P_r(\frac{1}{24}\kappa(B^*\mathcal{H}(1-\varphi)^{1.25}D_a-4)\tau_2-\frac{1}{144}\kappa\Re A^*(1-\varphi)^{2.5}\tau_2)(-\frac{\kappa^2A^*P_r\tau_2\ell_o}{B^*}-$$

$$\frac{P_r E_c\left(4\kappa^2\tau_2+\tau_2^2\right)}{\Re B^*(1-\varphi)^{2.5}}-\frac{P_r E_c \mathcal{H}\tau_2}{B^*}))-\frac{1}{B^*}(\frac{1}{540}\kappa^3 A^{*2}P_r\Re(1-\varphi)^{2.5}\tau_2^2(-2\kappa^2\ell_o-\frac{\kappa^2 A^* P_r\ell_o}{B^*}-\frac{2\kappa^2 P_r E_c}{\Re B^*(1-\varphi)^{2.5}}-\frac{1}{2}\frac{P_r E_c\mathcal{H}}{B^*}-\frac{1}{2}\xi\ell_o))+\frac{1}{\Re B^*(1-\varphi)^{2.5}}(\frac{1}{9}P_r E_c(4\kappa^2(\frac{1}{120}\kappa\Re A^*(1-\varphi)^{2.5}\tau_2^3+\left(\frac{1}{24}\kappa(B^*\mathcal{H}(1-\varphi)^{1.25}D_a-4)\tau_2-\frac{1}{12}\kappa\Re A^*(1-\varphi)^{2.5}\tau_2\right)^2)-\frac{1}{10}(\frac{1}{6}\kappa(B^*\mathcal{H}(1-\varphi)^{1.25}D_a-4)\tau_2-\frac{1}{3}\kappa\Re A^*(1-\varphi)^{2.5}\tau_2)\kappa\Re A^*(1-\varphi)^{2.5}\tau_2^2))+\frac{1}{B^*}(\frac{1}{9}P_r E_c\mathcal{H}(-\frac{1}{120}\kappa\Re A^*(1-\varphi)^{2.5}\tau_2^3+(\frac{1}{24}(B^*\mathcal{H}(1-\varphi)^{1.25}D_a-4)\tau_2-\frac{1}{12}\kappa\Re A^*(1-\varphi)^{2.5}\tau_2)^2)))]\kappa^{10}-[\frac{1}{12}(\frac{1}{B^*}(\kappa^2 A^* P_r(\frac{1}{24}\kappa(B^*\mathcal{H}(1-\varphi)^{1.25}D_a-4)\tau_2-\frac{1}{12}\kappa\Re A^*(1-\varphi)^{2.5}\tau_2)(-\frac{1}{30}\frac{\kappa^2 P_r E_c\tau_2^2}{\Re B^*(1-\varphi)^{2.5}}-\frac{1}{120}\frac{P_r E_c\mathcal{H}\tau_2^2}{B^*}))-\frac{1}{B^*}(\frac{1}{7920}\kappa^3 A^{*2}P_r\Re(1-\varphi)^{2.5}\tau_2^2(-\frac{\kappa^2 A^* P_r\tau_2\ell_o}{B^*}-\frac{P_r E_c\left(4\kappa^2\tau_2+\tau_2^2\right)}{\Re B^*(1-\varphi)^{2.5}}-\frac{P_r E_c\mathcal{H}\tau_2}{B^*}))+\frac{1}{\Re B^*(1-\varphi)^{2.5}}(\frac{1}{11}P_r E_c(-\frac{1}{15}\kappa^3(\frac{1}{24}\kappa(B^*\mathcal{H}(1-\varphi)^{1.25}D_a-4)\tau_2-\frac{1}{12}\kappa\Re A^*(1-\varphi)^{2.5}\tau_2)\Re A^*(1-\varphi)^{2.5}\tau_2^2+\frac{1}{400}\kappa^2 A^{*2}\Re^2(1-\varphi)^5\tau_2^4-\frac{1}{B^*}(\frac{1}{660}P_r E_c\mathcal{H}(\frac{1}{24}\kappa(B^*\mathcal{H}(1-\varphi)^{1.25}D_a-4)\tau_2-\frac{1}{12}\kappa\Re A^*(1-\varphi)^{2.5}\tau_2)\kappa\Re A^*(1-\varphi)^{2.5}\tau_2^2)]\kappa^{12}-0.07142857143[-\frac{1}{B^*}(\frac{641}{500000}\kappa^3 A^{*2}P_r\Re(1-\varphi)^{2.5}\tau_2^2(-\frac{1}{30}\frac{\kappa^2 P_r E_c\tau_2^2}{\Re B^*(1-\varphi)^{2.5}}-\frac{1}{120}\frac{P_r E_c\mathcal{H}\tau_2^2}{B^*}))+\frac{21367}{10000}\frac{\kappa^4 A^{*2}P_r E_c\Re(1-\varphi)^{2.5}\tau_2^4}{B^*}+\frac{53418}{100000}\frac{\kappa^2 A^{*2}P_r E_c\mathcal{H}\Re^2(1-\varphi)^{2.5}\tau_2^4}{B^*}]\kappa^{14} \quad (39)$$

4. Results and Discusses

In this section, we will present tables, charts, and drawings that discuss the increase and decrease, as well as the approximate analysis of the mentioned method, as shown below. This section discusses the results of the flow and heat transfer analysis. The flow and heat transfer through a diverging/converging channel with a porous medium are depicted here at constant parametric values for physical parameters. The behaviour of physical parameters as well as their values in density, specific heat, thermal conductivity, and electrical conductivity, where (ξ): The heat generation/absorption Parameter is non-dimensional and depends on the amount of heat generated or absorbed in the fluid. (κ), the flow between two planes that meet at an angle, (ν) the viscous flow equation describes accurately the flow conditions for a relatively small range corresponding to low Reynolds numbers. Such flows are characterized by layers of fluid gliding over each other near solid boundaries. ($K_{n.f}$) The kinematic viscosity is defined as the absolute viscosity of a liquid divided by its density at the same temperature. As an example biodiesel presents greater viscosity than diesel due to a higher degree of unsaturation and by oxidation reactions that can modify the fatty acid composition during storage, transportation, and temperature change. Viscous flow takes place when there is a crack or a defect into membrane structure and gases can pass through the membrane without separation. ($\Re$), it is a dimensionless quantity in fluid mechanics that helps predict fluid flow patterns in different situations by measuring the ratio between inertial forces and viscous forces. Whereas at lower Reynolds numbers the flows tend to be dominated by laminar flow, while at higher Reynolds numbers the flows tend to be turbulent. ($\mathcal{H}$), it is the ratio of the electromagnetic force to the viscous force, (P_r) is a dimensionless number, the ratio of momentum diffusivity to thermal diffusivity, (E_c) is a dimensionless number used in continuum mechanics. It expresses the relationship between a flow's kinetic energy and the boundary layer enthalpy difference, and is used to characterize heat transfer dissipation. (φ), the ratio of the volume of a constituent to the volume of

the whole. In practice, it may be difficult to determine the volume fraction because differences in the molecular sizes of the constituents may produce a total volume that differs from the sum of the in dividual volumes of the mixture. When materials of similar physio chemical characteristics (such as multiple aqueous solutions) are combined this is not a problem. As shown in Table 1, the convergence values for the nanoparticle materials $Cu, Ag, Al_2O_3, and\ TiO_2$ at $\varphi = 0.01$ and various values of $\Re, \mathcal{H}, P_r, E_c$ and κ, at both converge/diverge channels are shown in Table 2-7. The Table 8–15 display the outcomes of applying various values for the four materials and demonstrate convergence in outcomes when compared with the Range–Kutta of fourth order (RK–4). Additionally, by comparing the residual error between the numerical method and the presented method, we discover a good reading and an excellent error rate. We observe in Table 16 that the impact of altering the values of P_r, E_c and ξ about the temperature profile when examining the produced absolute values, we discover that the increase is linear, with higher values indicating a direct increase of P_r, E_c and ξ, the temperature profile values of Cu material increase. In Table 17, we discussed the effect of the difference of the Reynolds number ($\Re$) and the Hartmann number ($\mathcal{H}$) on the temperature profile and the velocity profile of the (Ag) material, where when taking the absolute values resulting from the various of the $\Re$, with an increase in the $\Re$ we notice a decrease in the values of both the velocity and temperature profiles, but an increase in the $\mathcal{H}$, leads to an increase in the velocity profile and temperature profile. In Table 18, the effect on each of the velocity and temperature profiles of the Al_2O_3material when various values of each of the Nanoparticle concentration (φ), and the Darcy number (D_a). An increase in the values of φ leads to an increase in the velocity and temperature profiles, and an increase in the (D_a), leads to a decrease in both the velocity and temperature profiles. This comparison takes place when take absolute values. Finally, in Table 19, when various the open angle (κ) of each of the diverging and converging channels, we notice a decrease in both the velocity and temperature profiles when taking the absolute value of the values for titanium.

Table 1
Physical parameter of nanoparticles materials

Material	Density (Kg/m^3)	Specific heat capacity (J/kgK)	Thermal conductivity (W/mk)	Electrical conductivity $(\Omega.m)^{-1}$
Water	997.1	4179	0.613	0.05
Copper	8933	385	401	5.96×10^7
silver	10500	235	429	6.3×10^7
Aluminum	3970	765	40	3.4×10^7
Titanium	4250	686.2	8.9538	2.38×10^6

Table 2
The convergence values for the nanoparticle material of Cu and Ag when $\varphi = 0.01$

Order	$\Re = 10, \mathcal{H} = 15$			
	$\kappa = 1^o$			
	Cu		Ag	
	τ_2	ℓ_o	τ_2	ℓ_o
Order[1]	-2.012224743	1.000665090	-2.138315311	1.000629000
Order[2]	-2.012242473	1.001399850	-2.135923140	1.001283927
Order[3]	-2.012242473	1.002056780	-2.135948805	1.001911396
Order[4]	-2.012242473	1.001896445	-2.135948633	1.002235595
Order[5]	-2.012242473	1.001362713	-2.135948633	1.002437234

Table 3
The convergence values for the nanoparticle material when $\varphi = 0.01$

Order	$\Re = 10, \mathcal{H} = 15$			
	$\kappa = -1^{o}$			
	Cu		Ag	
	τ_2	ℓ_o	τ_2	ℓ_o
Order[1]	-1.987787217	1.000665266	-1.987794735	1.000665266
Order[2]	-1.987804151	1.001399656	-1.987811675	1.001399655
Order[3]	-1.987804152	1.002055991	-1.987811676	1.002055991
Order[4]	-1.987804152	1.001909112	-1.987811676	1.001909109
Order[5]	-1.987804152	1.001381777	-1.987811676	1.001381776

Table 4
The convergence values for the nanoparticle material when $\varphi = 0.01$

Order	$\Re = 50, \mathcal{H} = 50$			
	$\kappa = 3^{o}$			
	Al_2O_3		TiO_2	
	τ_2	ℓ_o	τ_2	ℓ_o
Order[1]	-2.27682822	1.00570190	-2.27670125	1.00570190
Order[2]	-2.27928547	1.01173035	-2.27916071	1.01173033
Order[3]	-2.27929357	1.01755397	-2.27916877	1.01755395
Order[4]	-2.27929407	1.01999921	-2.27916927	1.01999946
Order[5]	-2.27929407	1.02123011	-2.27916927	1.02123050

Table 5
The convergence values for the nanoparticle material when $\varphi = 0.01$

Order	$\Re = 50, \mathcal{H} = 50$			
	$\kappa = -3^{o}$			
	Al_2O_3		TiO_2	
	τ_2	ℓ_o	τ_2	ℓ_o
Order[1]	-1.74842081	1.00571588	-1.74851569	1.00571587
Order[2]	-1.74637522	1.01171349	-1.74647561	1.01171348
Order[3]	-1.74637488	1.01750100	-1.74647533	1.01750099
Order[4]	-1.74637511	1.02096935	-1.74647556	1.02096918
Order[5]	-1.74637511	1.02273433	-1.74647556	1.02273411

Table 6
The convergence values for the nanoparticle material when $\varphi = 0.01$

Order	$\Re = 10, \mathcal{H} = 10$			
	$\kappa = 5^{o}$			
	Cu		TiO_2	
	τ_2	ℓ_o	τ_2	ℓ_o
Order[1]	-2.140303425	1.015548388	-2.140607552	1.015548461
Order[2]	-2.138924673	1.031648435	-2.139220784	1.031648669
Order[3]	-2.138937129	1.048225856	-2.139233345	1.048226099
Order[4]	-2.138937070	1.064215609	-2.139233285	1.064215359
Order[5]	-2.138937070	1.078853067	-2.139233285	1.078851629

Table 7
The convergence values for the nanoparticle material when $\varphi = 0.01$

Order	$\Re = 10, \mathcal{H} = 10$			
	$\kappa = -5^{o}$			
	Cu		TiO_2	
	τ_2	ℓ_o	τ_2	ℓ_o
Order[1]	-1.870300818	1.015551323	-1.870046681	1.015551405
Order[2]	-1.868803052	1.031642939	-1.868540967	1.031643157
Order[3]	-1.868790736	1.048227799	-1.868528551	1.048228057
Order[4]	-1.868790671	1.064354891	-1.868528486	1.064354982
Order[5]	-1.868790671	1.079164690	-1.868528486	1.079164119

Table 8
The results of velocity and temperature profiles for Cu and comparing with Range-Kutta of forth order at $\varphi = 0.01$

$\varkappa$	$\Re = 10, \mathcal{H} = 15$					
	$\kappa = 1^{o}$					
	Cu					
	$\hbar(\varkappa)$	RK~4	Residual error	$\Theta(\varkappa)$	RK~4	Residual error
0.00	1.0000000000	1.000000000	0.000000000	1.000665090	1.000665090	0.000000000
0.10	0.9899400507	0.989940056	5.3×10^{-9}	1.000658245	1.000658246	1×10^{-9}
0.20	0.9597740233	0.959774043	1.9×10^{-8}	1.000637739	1.000637741	2×10^{-9}
0.30	0.9095413309	0.909541349	1.8×10^{-8}	1.000603658	1.000603665	7×10^{-9}
0.40	0.8393007561	0.839300835	7.8×10^{-8}	1.000556140	1.000556159	1.9×10^{-8}
0.50	0.7491206055	0.749120200	4.0×10^{-7}	1.000495362	1.000495409	4.7×10^{-8}
0.60	0.6390625195	0.639063583	1.0×10^{-6}	1.000421536	1.000421631	9.5×10^{-8}
0.70	0.5091691507	0.509167254	1.8×10^{-6}	1.000334885	1.000335057	1.7×10^{-7}
0.80	0.3594305973	0.359428524	2.0×10^{-6}	1.000235628	1.000235916	2.8×10^{-7}
0.90	0.1897684996	0.189768944	4.4×10^{-7}	1.000123954	1.000124412	4.5×10^{-7}
1.00	0.0000000000	0.000009441	0.000000000	1.000000000	1.000000696	0.000000000

Table 9
The results of velocity and temperature profiles for Ag and comparing with Range-Kutta of forth order at $\varphi = 0.01$

$\varkappa$	$\Re = 30, \mathcal{H} = 15$					
	$\kappa = 3^{o}$					
	Ag					
	$\hbar(\varkappa)$	RK~4	Residual error	$\Theta(\varkappa)$	RK~4	Residual error
0.00	1.0000000000	1.0000000000	0.00000000	1.005580663	1.005580663	0.000000000
0.10	0.9883329368	0.9883330055	6.8×10^{-8}	1.005524592	1.005524594	2.0×10^{-9}
0.20	0.9536134423	0.9536127808	6.6×10^{-7}	1.005356420	1.005356429	9.0×10^{-9}
0.30	0.8966617186	0.8966500537	1.1×10^{-5}	1.005076261	1.005076305	4.4×10^{-8}
0.40	0.8187618246	0.8186964324	6.5×10^{-5}	1.004684305	1.004684436	1.3×10^{-7}
0.50	0.7215372593	0.7213065874	2.3×10^{-4}	1.004180793	1.004181099	3.0×10^{-7}
0.60	0.6067767767	0.6061657731	6.1×10^{-4}	1.003566013	1.003566619	6.0×10^{-7}
0.70	0.4762104361	0.4748976135	1.3×10^{-3}	1.002840267	1.002841348	1.0×10^{-6}
0.80	0.3312358846	0.3288649603	2.3×10^{-3}	1.002003855	1.002005642	1.7×10^{-7}
0.90	0.1725948722	0.1689717473	3.6×10^{-3}	1.001057036	1.001059838	2.8×10^{-6}
1.00	0.0000000000	0.0000000000	0.00000000	1.000000000	1.000000000	0.0000000000

Table 10
The results of velocity and temperature profiles for Cu and comparing with Range-Kutta of forth order at $\varphi = 0.01$

$\varkappa$	$\Re = 10, \mathcal{H} = 15$					
	$\kappa = -1^{o}$					
	Cu					
	$\hbar(\varkappa)$	RK~4	Residual error	$\Theta(\varkappa)$	RK~4	Residual error
0.00	1.0000000000	1.0000000000	0.00000000	1.000665266	1.000665266	0.000000000
0.10	0.9900599037	0.9900598981	5.6×10^{-9}	1.000658421	1.000658422	1.0×10^{-9}
0.20	0.9602259580	0.9602259510	5.1×10^{-9}	1.000637915	1.000637917	2.0×10^{-9}
0.30	0.9104591917	0.9104591089	8.2×10^{-8}	1.000603833	1.000603839	6.0×10^{-9}
0.40	0.8407013147	0.8407010571	2.5×10^{-7}	1.000556308	1.000556328	2.0×10^{-8}
0.50	0.7508847113	0.7508840277	6.8×10^{-7}	1.000495521	1.000495569	4.8×10^{-8}
0.60	0.6409464302	0.6409449630	1.4×10^{-6}	1.000421679	1.000421778	9.9×10^{-8}
0.70	0.5108461726	0.5108437141	2.2×10^{-6}	1.000335004	1.000335189	1.8×10^{-7}
0.80	0.3605882772	0.3605854277	2.4×10^{-6}	1.000235714	1.000236031	3.1×10^{-7}
0.90	0.1902477008	0.1902470674	6.3×10^{-7}	1.000124000	1.000124508	5.0×10^{-7}
1.00	0.0000000000	0.0000000000	0.00000000	1.000000000	1.000000000	0.0000000000

Table 11
The results of velocity and temperature profiles for Ag and comparing with Range-Kutta of forth order at $\varphi = 0.01$

$\varkappa$	$\Re = 30, \mathcal{H} = 15$					
	$\kappa = -1^{o}$					
	Ag					
	$\hbar(\varkappa)$	RK~4	Residual error	$\Theta(\varkappa)$	RK~4	Residual error
0.00	1.0000000000	1.0000000000	0.000000000	1.005586407	1.005586407	0.000000000
0.10	0.9913629754	0.9913629378	3.7×10^{-8}	1.005530335	1.005530337	1×10^{-9}
0.20	0.9652434077	0.9652425589	8.4×10^{-7}	1.005362148	1.005362160	12×10^{-8}
0.30	0.9210293418	0.9210196899	9.6×10^{-6}	1.005081934	1.005081981	47×10^{-8}
0.40	0.8577459408	0.8576936947	5.2×10^{-5}	1.004689833	1.004689978	1.5×10^{-7}
0.50	0.7741231184	0.7739359585	1.8×10^{-4}	1.004186031	1.004186391	3.6×10^{-7}
0.60	0.6686902243	0.6681776595	5.1×10^{-4}	1.003570754	1.003571521	7.7×10^{-7}
0.70	0.5398977818	0.5387441910	1.5×10^{-3}	1.002844253	1.002845713	1.5×10^{-6}
0.80	0.3862662800	0.3840506640	2.2×10^{-3}	1.002006792	1.002009342	2.5×10^{-6}
0.90	0.2065620179	0.2028725979	3.6×10^{-3}	1.001058629	1.001062789	4.2×10^{-5}
1.00	0.0000000000	0.0000000000	0.000000000	1.000000000	1.000000000	0.000000000

Table 12
The results of velocity and temperature profiles for Al_2O_3 and comparing with Range-Kutta of forth order at $\varphi = 0.01$

$\varkappa$	$\Re = 50, \mathcal{H} = 50$					
	$\kappa = 3^o$					
	Al_2O_3					
	$\hbar(\varkappa)$	RK~4	Residual error	$\Theta(\varkappa)$	RK~4	Residual error
0.00	1.0000000000	1.0000000000	0.00000000	1.005701908	1.005701908	0.000000000
0.10	0.9886405318	0.9886406412	1.0×10^{-7}	1.005644138	1.005644138	0.000000000
0.20	0.9548529497	0.9548523634	5.8×10^{-7}	1.005470943	1.005470950	7.0×10^{-9}
0.30	0.8994703346	0.8994582712	1.2×10^{-5}	1.005182662	1.005182699	3.7×10^{-8}
0.40	0.8237498646	0.8236838979	6.5×10^{-5}	1.004779831	1.004779940	1.0×10^{-7}
0.50	0.7291758795	0.7289561317	2.1×10^{-4}	1.004263152	1.004263386	2.3×10^{-7}
0.60	0.6171841711	0.6166526325	5.3×10^{-4}	1.003633436	1.003633855	4.1×10^{-7}
0.70	0.4888074995	0.4878208547	9.8×10^{-4}	1.002891533	1.002892204	6.7×10^{-7}
0.80	0.3442423356	0.3428778096	1.3×10^{-3}	1.002038253	1.002039268	1.0×10^{-6}
0.90	0.1823368284	0.1812877158	1.0×10^{-3}	1.001074270	1.001075798	1.5×10^{-6}
1.00	0.0000000000	0.0000000000	0.00000000	1.000000000	1.000000000	0.00000000

Table 13
The results of velocity and temperature profiles for TiO_2 and comparing with Range-Kutta of forth order at $\varphi = 0.01$

$\varkappa$	$\Re = 50, \mathcal{H} = 50$					
	$\kappa = 3^o$					
	TiO_2					
	$\hbar(\varkappa)$	RK~4	Residual error	$\Theta(\varkappa)$	RK~4	Residual error
0.00	1.0000000000	1.0000000000	0.000000000	1.005701907	1.005701907	0.00000000
0.10	0.9886411572	0.9886412666	$1.\times 10^{-7}$	1.005644137	1.005644137	0.00000000
0.20	0.9548553408	0.9548547551	5.8×10^{-7}	1.005470942	1.005470949	1×10^{-9}
0.30	0.8994753098	0.8994632554	1.2×10^{-5}	1.005182661	1.005182698	3.7×10^{-8}
0.40	0.8237577427	0.8236918246	$6.\times 10^{-5}$	1.004779831	1.004779939	1.0×10^{-7}
0.50	0.7291863564	0.7289667740	$2.\times 10^{-4}$	1.004263152	1.004263386	2.3×10^{-7}
0.60	0.6171962736	0.6166651521	$5.\times 10^{-4}$	1.003633435	1.003633856	4.2×10^{-7}
0.70	0.4888196376	0.4878338267	$9.\times 10^{-4}$	1.002891533	1.002892206	6.7×10^{-7}
0.80	0.3442524742	0.3428892923	1.1×10^{-3}	1.002038253	1.002039270	1.0×10^{-6}
0.90	0.1823428043	0.1812953440	1.0×10^{-3}	1.001074270	1.001075800	1.5×10^{-6}
1.00	0.0000000000	0.0000000000	0.000000000	1.000000000	1.000000000	0.00000000

Table 14
The results of velocity and temperature profiles for $Al_2O_3$and comparing with Range-Kutta of forth order at $\varphi = 0.01$

$\varkappa$	$\Re = 50, \mathcal{H} = 50$					
	$\kappa = -3^o$					
	Al_2O_3					
	$\hbar(\varkappa)$	RK~4	Residual error	$\Theta(\varkappa)$	RK~4	Residual error
0.00	1.0000000000	1.0000000000	0.000000000	1.005715886	1.005715886	0.000000000
0.10	0.9912389297	0.9912388651	6.4×10^{-8}	1.005658113	1.005658114	1×10^{-9}
0.20	0.9647312204	0.9647301655	1.0×10^{-6}	1.005484882	1.005484892	1×10^{-8}
0.30	0.9198266038	0.9198156340	1.0×10^{-5}	1.005196457	1.005196505	4.8×10^{-7}
0.40	0.8555187209	0.8554620006	5.6×10^{-5}	1.004793256	1.004793418	1.6×10^{-7}
0.50	0.7705612556	0.7703684985	1.9×10^{-4}	1.004275839	1.004276264	4.2×10^{-7}
0.60	0.6636305201	0.6631397145	4.9×10^{-4}	1.003644870	1.003645812	9.4×10^{-7}
0.70	0.5335344942	0.5325426473	9.9×10^{-4}	1.002901082	1.002902929	1.8×10^{-6}
0.80	0.3794683178	0.3778651182	1.9×10^{-3}	1.002045220	1.002048519	3.2×10^{-6}
0.90	0.2013162369	0.1993822407	1.9×10^{-3}	1.001077993	1.001083433	5.4×10^{-6}
1.00	0.0000000000	0.0000000000	0.000000000	1.000000000	1.000000000	0.000000000

Table 15
The results of velocity and temperature profiles for $TiO_2$and comparing with Range-Kutta of forth order at $\varphi = 0.01$

$\varkappa$	$\Re = 50, \mathcal{H} = 50$					
	$\kappa = -3^o$					
	TiO_2					
	$\hbar(\varkappa)$	RK~4	Residual error	$\Theta(\varkappa)$	RK~4	Residual error
0.00	1.0000000000	1.0000000000	0.000000000	1.005715879	1.005715879	0.00000000
0.10	0.9912384603	0.9912383959	6.4×10^{-8}	1.005658106	1.005658107	1.0×10^{-9}
0.20	0.9647294044	0.9647283502	1.0×10^{-6}	1.005484875	1.005484885	1.0×10^{-8}
0.30	0.9198227460	0.9198117830	1.0×10^{-5}	1.005196450	1.005196499	4.9×10^{-8}
0.40	0.8555124256	0.8554557411	5.6×10^{-5}	1.004793249	1.004793412	1.6×10^{-7}
0.50	0.7705525364	0.7703599069	1.9×10^{-4}	1.004275833	1.004276258	4.2×10^{-7}
0.60	0.6636199012	0.6631294428	4.9×10^{-4}	1.003644866	1.003645806	9.4×10^{-7}
0.70	0.5335230986	0.5325320234	9.9×10^{-4}	1.002901077	1.002902924	1.8×10^{-6}
0.80	0.3794579414	0.3778561880	1.6×10^{-3}	1.002045217	1.002048515	3.2×10^{-6}
0.90	0.2013094037	0.1993777053	1.9×10^{-3}	1.001077991	1.001083430	5.4×10^{-6}
1.00	0.0000000000	0.0000000000	0.00000000	1.000000000	1.000000000	0.000000000

Table 16
Variation in $\frac{d\Theta(1)}{d\varkappa}$ with varying $P_r, E_c and\ \xi$ when $\Re = 30, \mathcal{H} = 25, \kappa = 1^o$ and $\varphi = 0.04$ for Cu

P_r	$\frac{d\Theta(1)}{d\varkappa}$	E_c	$\frac{d\Theta(1)}{d\varkappa}$	ξ	$\frac{d\Theta(1)}{d\varkappa}$
0.1	-0.00705864823	0.1	-0.0474297702	0.1	-0.272329924
0.5	-0.02546210306	0.5	-0.2273333328	0.5	-1.282357059
0.7	-0.03462516897	0.7	-0.3172851142	0.7	-2.034040955
0.9	-0.04376251138	0.9	-0.4072368952	0.9	-3.035099216

Table 17
Variation in $\frac{\mathrm{d}\hbar(1)}{\mathrm{d}\varkappa}$ and $\frac{\mathrm{d}\Theta(1)}{\mathrm{d}\varkappa}$ with varying $\Re$ and $\mathcal{H}$ when $P_r = 0.01, E_c = 0.001, \kappa = 1^o$ and $\varphi = 0.04$ for Ag

$\Re$	$\frac{d\hbar(1)}{d\varkappa}$	$\frac{d\Theta(1)}{d\varkappa}$	$\mathcal{H}$	$\frac{d\hbar(1)}{d\varkappa}$	$\frac{d\Theta(1)}{d\varkappa}$
30	-1.975120129	-0.002903634606	30	-1.990634043	-0.002994687629
50	-1.914490763	-0.002899162416	50	-2.052207818	-0.003361734892
70	-1.853731605	-0.002893812489	70	-2.112939752	-0.003732622214
100	-1.762555091	-0.002884068494	100	-2.2-2274227	-0.004294359156

Table 18
Variation in $\frac{\mathrm{d}\hbar(1)}{\mathrm{d}\varkappa}$ and $\frac{\mathrm{d}\Theta(1)}{\mathrm{d}\varkappa}$ with varying φ, D_a and when $\Re = 30, \mathcal{H} = 25$, $P_r = 0.01, E_c = 0.001, \kappa = 1^o$ and $\varphi = 0.04$ for Al_2O_3

φ	$\frac{d\hbar(1)}{d\varkappa}$	$\frac{d\Theta(1)}{d\varkappa}$	D_a	$\frac{d\hbar(1)}{d\varkappa}$	$\frac{d\Theta(1)}{d\varkappa}$
0.1	-1.998970567	-0.002832272360	0.1	-2.610348384	-0.002921400176
0.5	-2.097927895	-0.002571960694	0.5	-2.052145775	-0.002907558576
0.7	-2.113577360	-0.002506068965	0.7	-2.008244551	-0.002905400925
0.9	-2.115800240	-0.002456475728	0.9	-1.983681768	-0.002904107772

Table 19
Variation in $\frac{\mathrm{d}\hbar(1)}{\mathrm{d}\varkappa}$ and $\frac{\mathrm{d}\Theta(1)}{\mathrm{d}\varkappa}$ with varying κ when $\Re = 30, \mathcal{H} = 25, P_r = 0.01, E_c = 0.001$ and $\varphi = 0.04$ for TiO_2

κ	$\frac{d\hbar(1)}{d\varkappa}$	$\frac{d\Theta(1)}{d\varkappa}$
-5^o	-2.131355431	-0.06622805050
-3^o	-2.077918650	-0.02302097556
3^o	-1.924611450	-0.02300030658
5^o	-1.875764598	-0.06616318441

Figure 2-7, illustrate different Prandtl values. The diagrams below show how each velocity file and temperature file behave when we use different values for the physical parameters, noting the increase and decrease in speed and temperature when using the analytical method used to produce good, efficient, and close results. Each of the diagrams below will be discussed in relation to its values and changes number.

This figure shows the behaviour of velocity profile and temperature profile when taken different values of Prandtl number and fixed other parameters ($\Re = 25, \mathcal{H} = 10, \varphi = 0.01, \kappa = 1^o$) it clears how it increasing in velocity profile and almost constant at temperature profile.

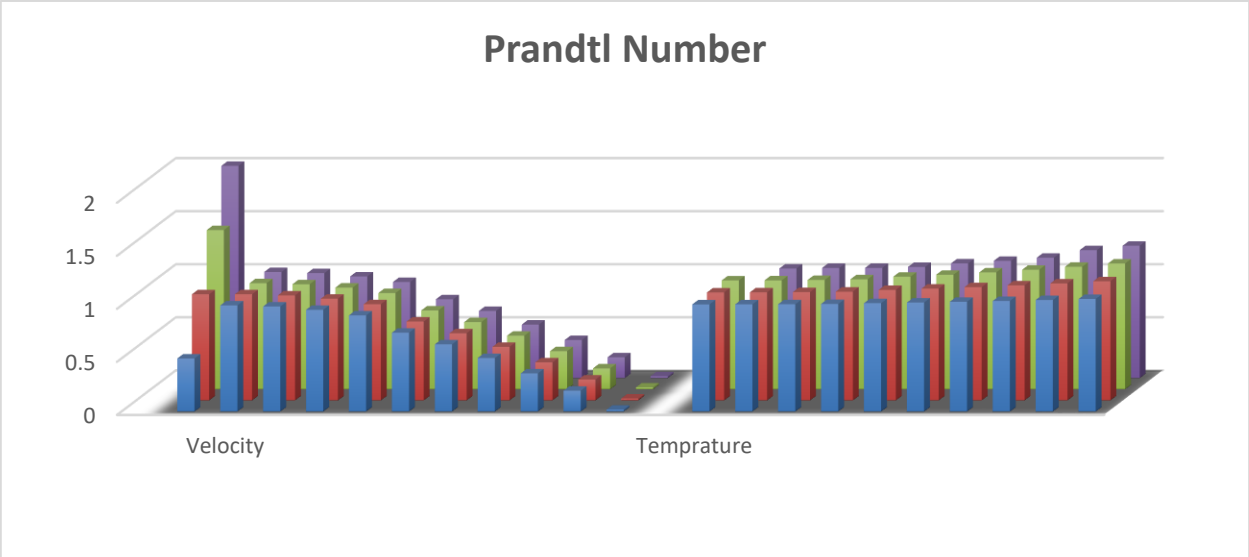

Fig. 2. Various Prandtl number values

At this figure the plane shows how the different values of Hartman number made the velocity profile decreasing and fixed in temperature profile when we take the values of physical parameter $(\Re = 25, \varphi = 0.01, \kappa = 1^o)$.

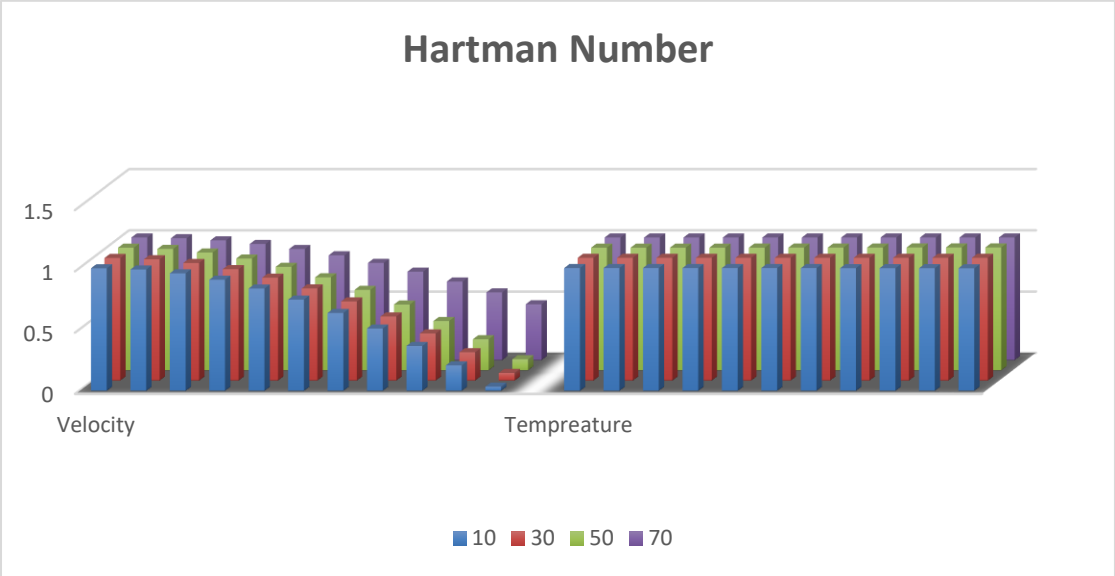

Fig. 3. Various Hartman number values

As seen in this figure when take a different values of nanoparticle volume fraction, the behaviour of velocity profile is decreasing and fixed along the temperature profile when $(\Re = 25, \mathcal{H} = 10, \kappa = 1^o)$.

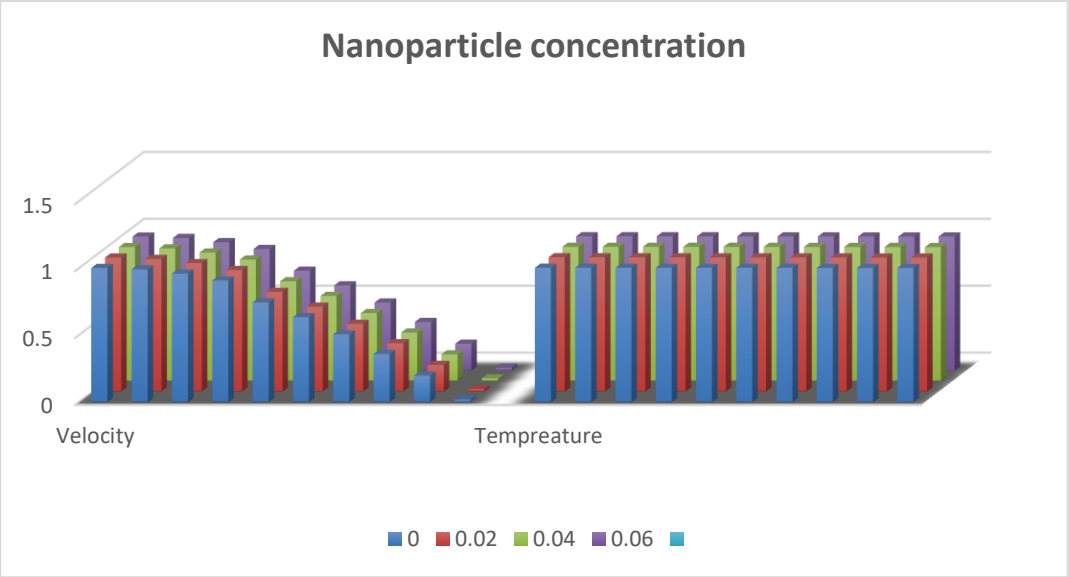

Fig. 4. Various nanoparticle volume fraction values

When take different values of Reynolds number there is an increasing in velocity profile as clear in plan above and fixed in temperature profile when $(\mathcal{H} = 10, \varphi = 0.01, \kappa = 1^o)$.

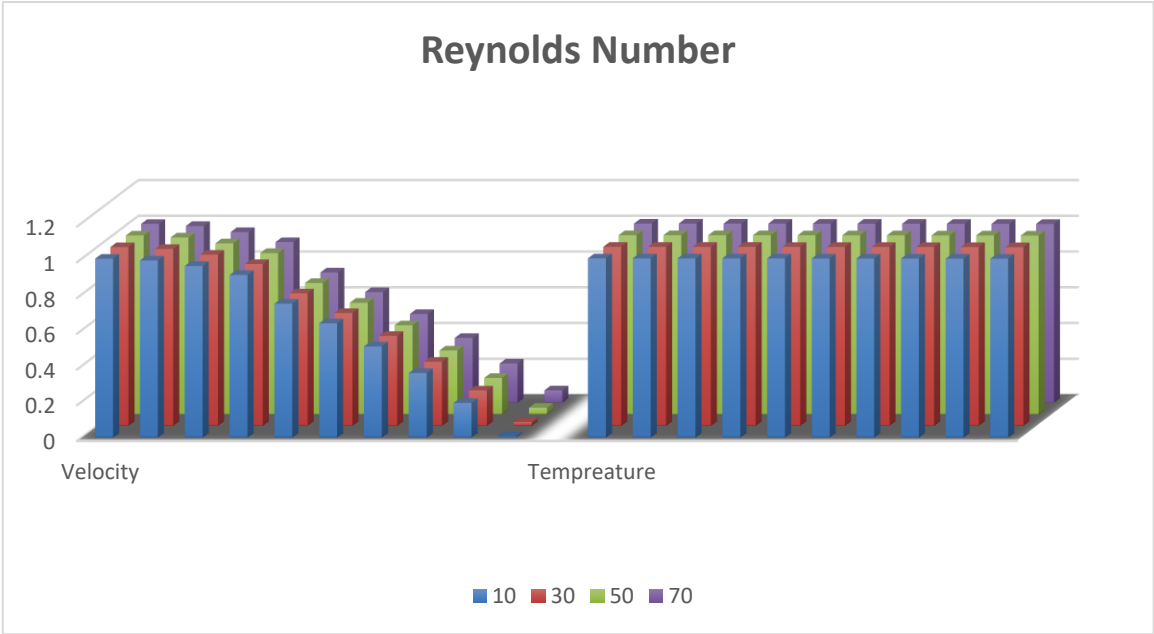

Fig. 5. Various Reynolds number values

At this plan when we take different values of Eckert number shows how the velocity profile are wobbling between increasing and decreasing, and the temperature profile was increasing clearly as shown above when $(\Re = 25, \mathcal{H} = 10, \varphi = 0.01, \kappa = 1^o)$.

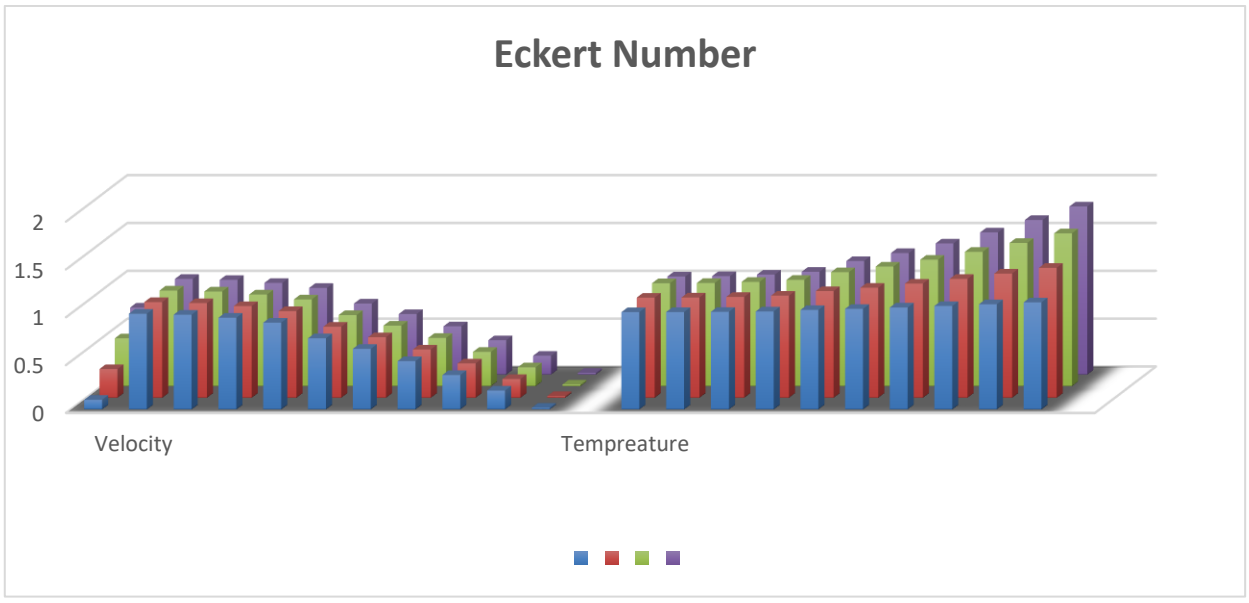

Fig. 6. Various Eckert number values

In this plan when take different type of open angle shows how increasing in both velocity and temperature profiles when $(\Re = 25, \mathcal{H} = 10, \varphi = 0.01)$.

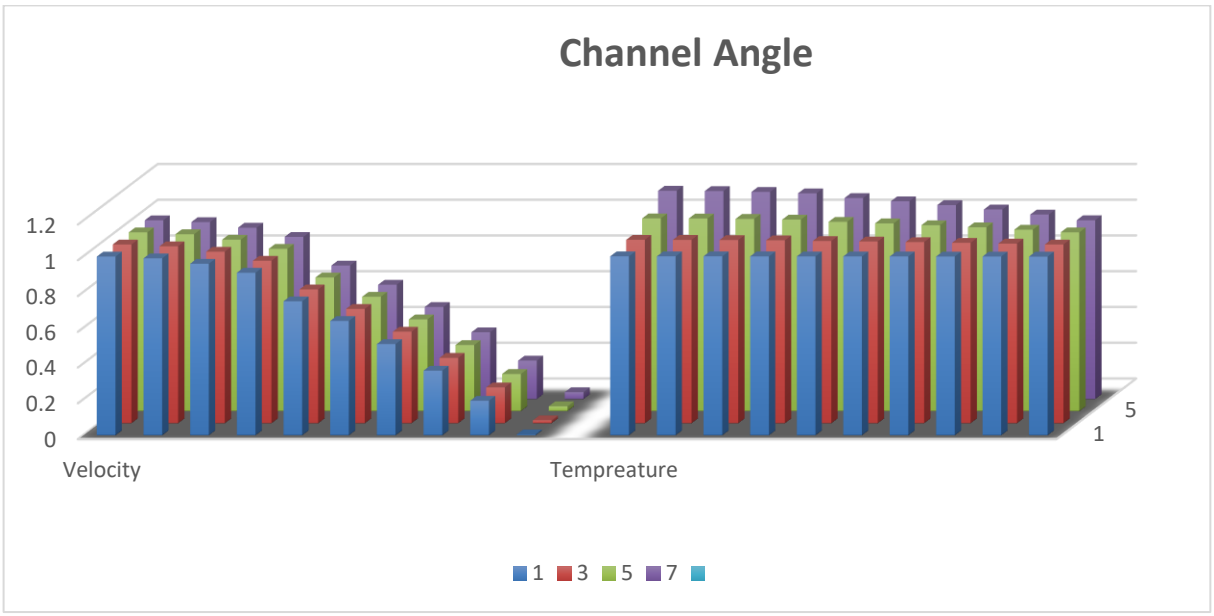

Fig. 7. Various open angle values

Figure 8-12, take many states of the four nanoparticle materials as shown where, Figure 8, see how increasing in velocity profile and temperature profile when we change in Reynolds number. Figure 9, shows increasing in velocity profile and temperature profile at different values of Hartman number. Figure 10, various values of nanoparticle concentration (φ) make increasing in velocity profile and temperature profile. Figure 11, shows increasing at temperature profiles when take different values of Prandtl and Eckert number. Figure 12, shows how temperature profile was decreasing at different values of Da, and increasing when take different values of ξ. Figure 13, shows the effective of channel angle on velocity profile and temperature profile, where it decreases and increases respectively.

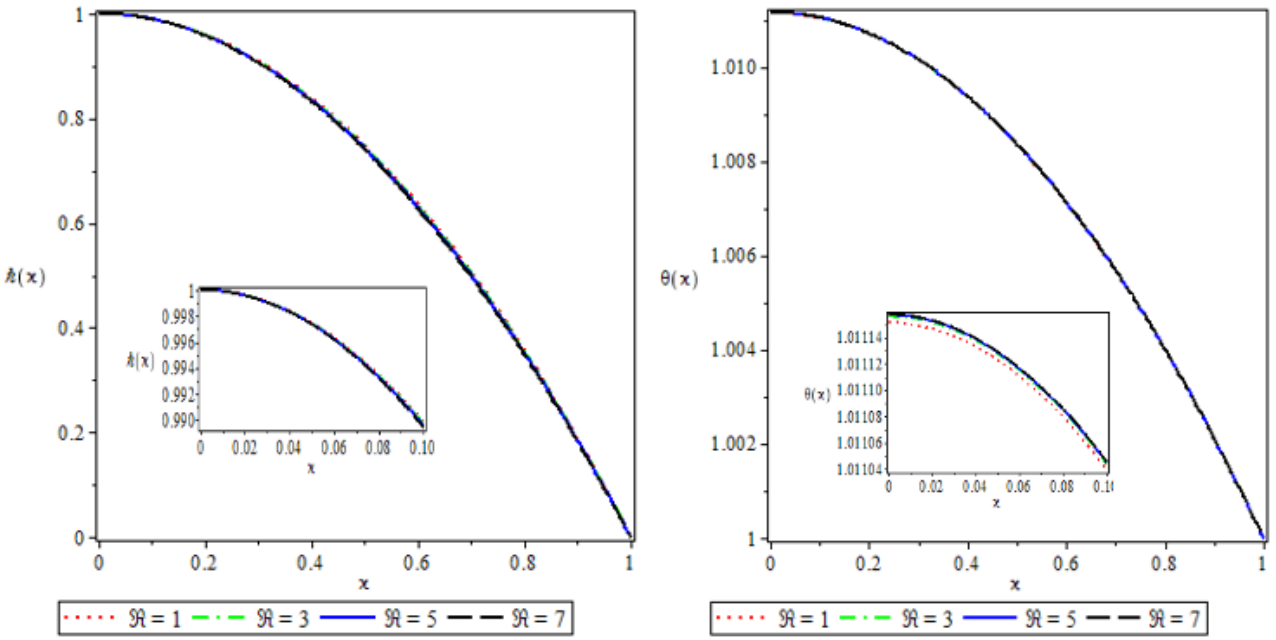

Fig. 8. Effect of Reynolds number normalized velocity profile and normalized temperature for nanoparticles nanofluid Cu when $\mathcal{H} = 2$, $\kappa = 3^o$, $\varphi = 0.01$

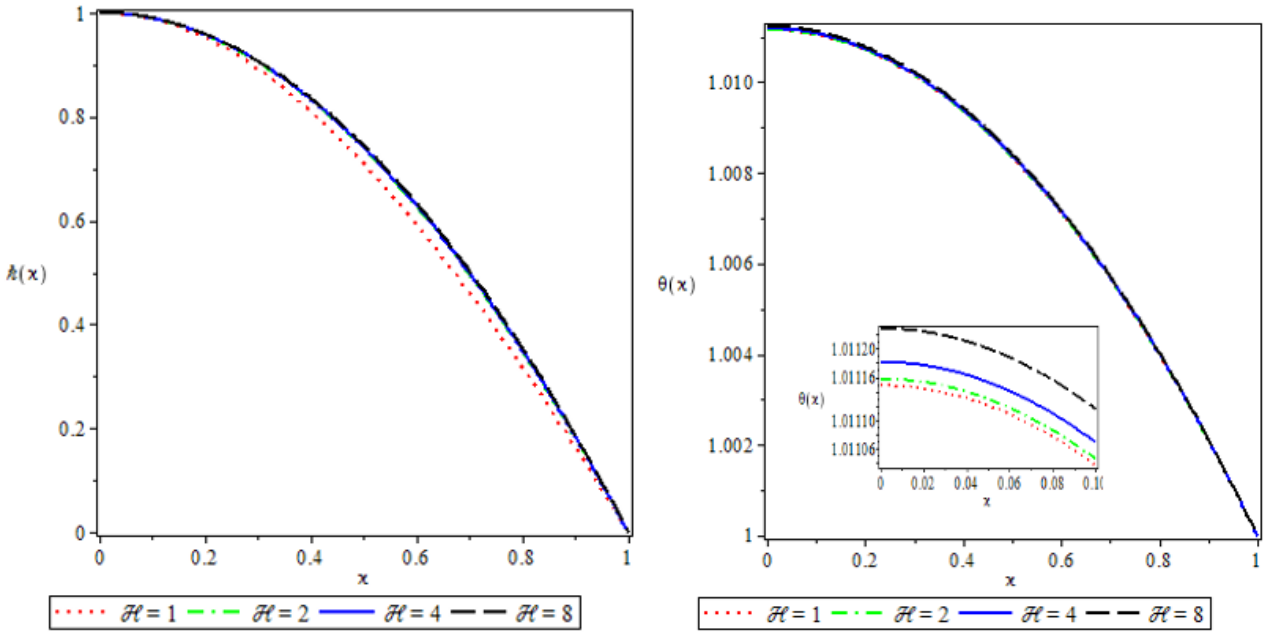

Fig. 9. Effect of Hartman number on normalized velocity profile and normalized temperature for nanoparticles nanofluid Cu when $\Re = 30$, $\kappa = 3^o$, $\varphi = 0.01$

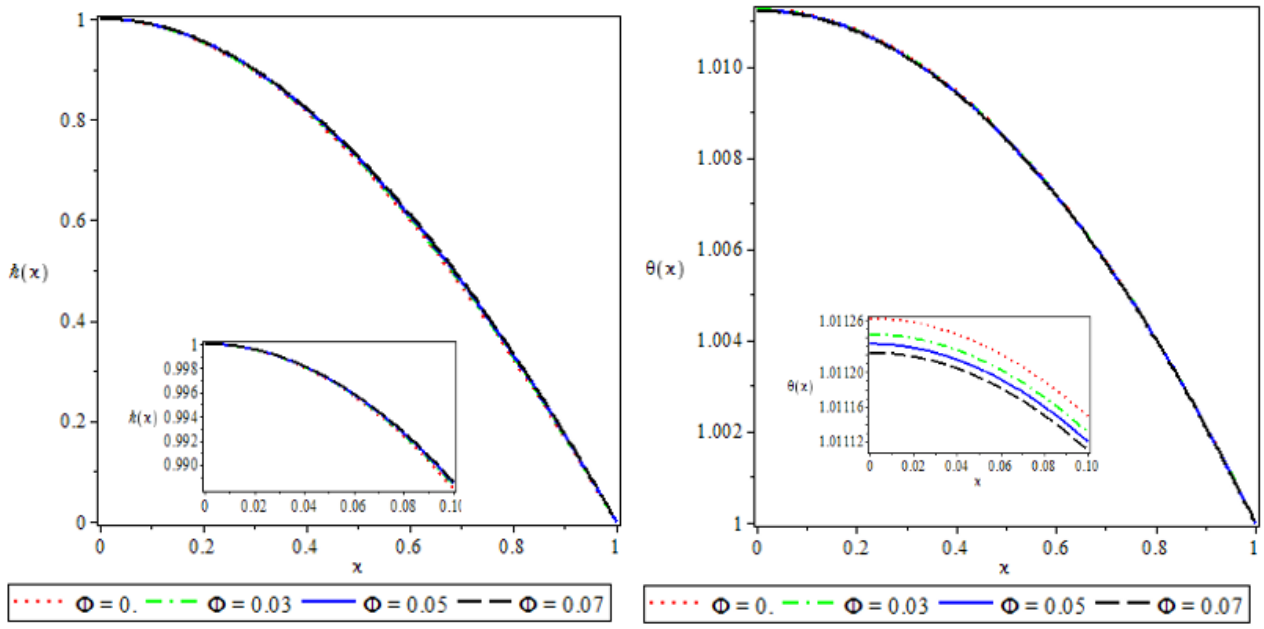

Fig. 10. Effect of nanoparticle concentration normalized velocity profile and normalized temperature for nanoparticles nanofluid Cu when $\mathcal{H} = 10$, $\Re = 30$, $\kappa = 3^o$

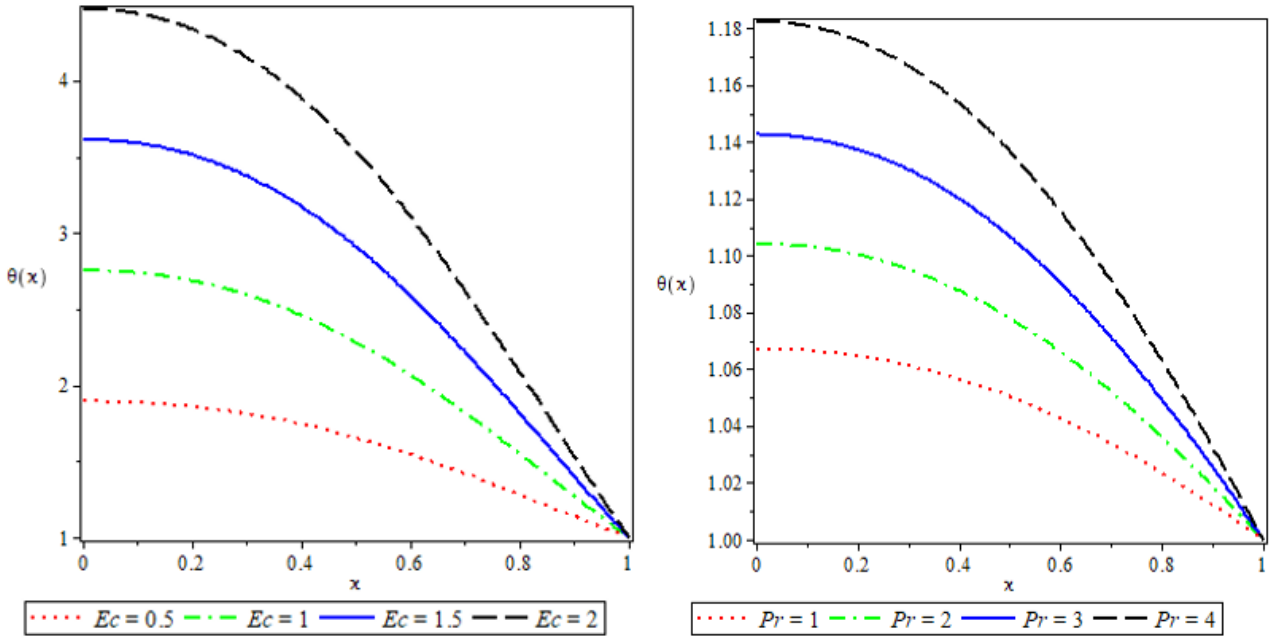

Fig. 11. Effect of Prandtl number and Eckert number on normalized temperature for nanoparticles nanofluid Cu when $\mathcal{H} = 15, \Re = 30$, $\kappa = 3^o$, $\varphi = 0.03$

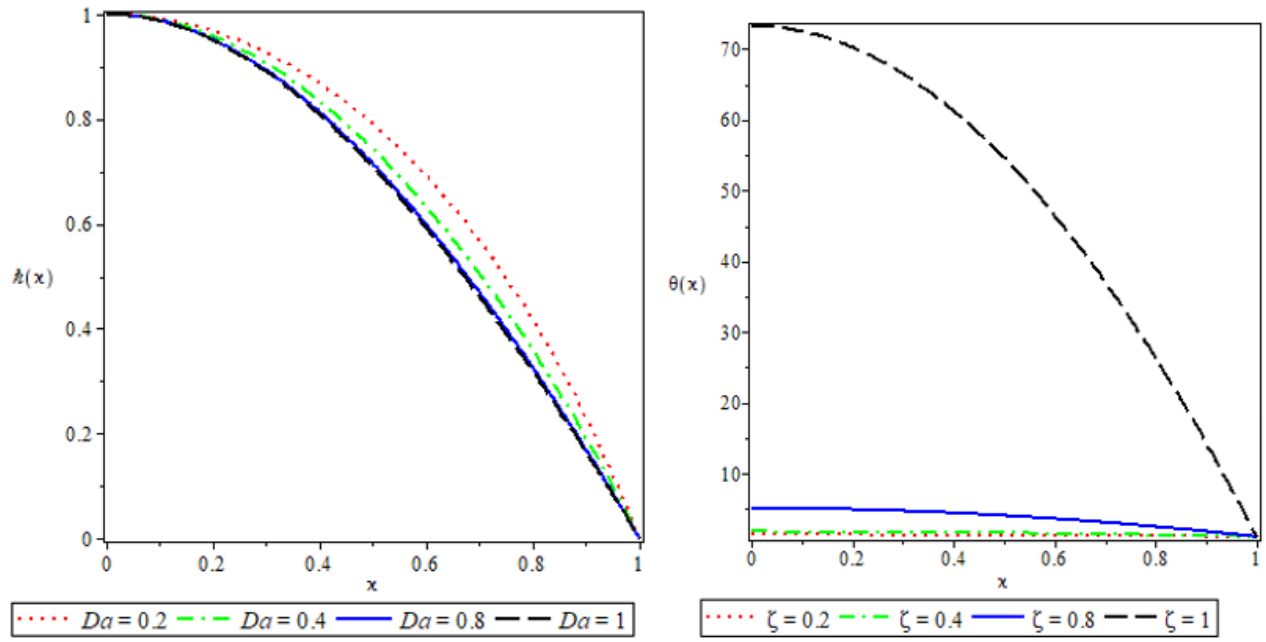

Fig. 12. Effect of Darcy number and Dimensionless heat generation parameter on Normalized temperature for nanoparticles nanofluid Cu when $\mathcal{H} = 15, \Re = 30$, $\kappa = 3^o$, $\varphi = 0.03$

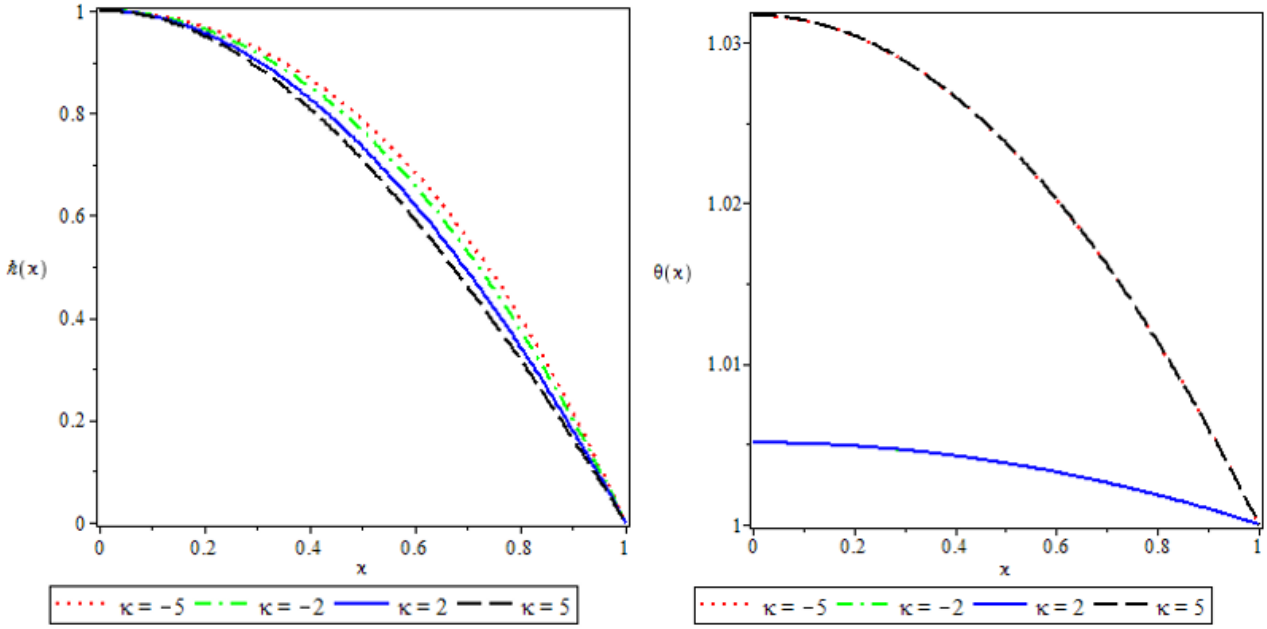

Fig. 13. Effect of channel angle on normalized velocity profile and normalized temperature for nanoparticles nanofluid Cu when $\mathcal{H} = 15, \Re = 30$, $\varphi = 0.03$.

Figure 10, depicts the effect of nanoparticle concentration (φ) on temperature distribution. This demonstrates that the addition of nanoparticles to fluid raises the temperature. The plot shows the heat transfer effect without nanoparticles through the Jeffery Hamel channel when φ is zero. As seen in Figure 8, increasing represents an improvement in the temperature distribution. The effect of Prandtl number (P_r) and Eckert number (E_c) on temperature is shown in Figure 11. As seen in the figures, the effect of (P_r) and (E_c) on heat transfer is significant. When the (P_r) and (E_c) parameter is increased, the kinematic viscosity becomes more dominant over the thermal diffusivity, implying a

larger momentum boundary layer than a thermal boundary layer. The effect of Darcy number (D_a) and Dimensionless heat generation parameter(ξ) on temperature distribution is shown in Figure 12, where temperature distribution decreases as D_a increases, and increases as (ξ) increases. Internal generated heat decreases due to decreased flow through the Jeffery Hamel channel as flow with porous media becomes obstructed as porosity increases. Temperature distribution decreases as Da decreases, as illustrated in the Figure 12. As a result, Table 6, shows the rate of approximation for the PIS's convergence. The numerical solution obtained by Runge-Kutta fourth order is used to validate the varying order of the approximate solution obtained using the PIS. The PIS solution improves with increasing order of approximation. Khan *et al.,* [57] demonstrates the solution for PIS convergence. By working in the PIS method on the usual non-linear Jeffrey Hamel equation and by looking at the results obtained in the tables and charts when controlling the values of physical parameters and showing full compatibility when comparing the presented method with a numerical method such as the fourth-order Range Kutta, as well as it can be said that this method is important for work In order to solve the turbulent flow problem of the Jeffrey Hamel equation, the tables show good agreement and excellent flow results in both divergent and convergent channels, that is, nanofluids with good viscosity and a certain density show good flow.

5. Conclusion

The effect of nanofluid flow through a converging/diverging channel with a porous medium on internally generated heat was investigated in this study. The momentum and energy equations were used to calculate the flow and heat transfer. Because most practical problems were nonlinear, the perturbation iteration scheme (PIS) was chosen as the appropriate method of analysis. In this work, the impacts of heat transfer on the Jeffery-Hamel nanofluid flow have been discussed. The collected findings demonstrate that PIS is an extremely handy, convenient, practical tool and strategy for obtaining a very precise solutions to nonlinear problems. Furthermore, the obtained solutions utilizing the proposed methodology were compared to approach numerical Range-Kutta of fourth order. PIS findings show a high level of agreement with numerical values. Working in this way gives us new solutions, starting with imposing new initial conditions with more constants to get results that have clear convergence and high accuracy that can be noticed when compared with other numerical methods previously studied on the same model in previous literature. The analytical results obtained in the presented tables indicate that they are fully compatible, and this appears when comparing them with the numerical methods and taking the error between them. Also, when displaying the diagrams and drawings and working on controlling the physical parameters, both the speed and temperature file indicate the good fluidity of the flow of nanofluids as well as the viscosity and density It takes a good turn in flow and ease of control when working practically in its applications. Also, the results of the analysis were used to investigate the effect of nanofluid rheology on transport performance. The obtained results show that

i. Reynolds number variation has a significant effect on fluid flow. The velocity of fluid transport is reduced when the Reynolds number is high.
ii. As the channel angle increases at the entrance, the flow at the exit decreases. iii. The effect of Darcy number on radial fluid velocity shows that fluid velocity decreases as it approaches the center plate, but fluid velocity increases as it approaches the center plate.
iii. Heat transfer analysis shows that as the Darcy number increases, the temperature decreases due to less flow through the channel. Blood flow through arteries and veins,

environmental flows through canals, molten polymer extrusion, and cold drawing operation through converging dies are all practical applications relevant to the study.

The future study of this method is done by expanding the horizons of working on nanofluids by taking fluids with higher densities. For example, we can replace water with oil or alcohol, or a mixture between oil and water, and so on, with different nanoparticles to obtain a more complex fluid and an advanced issue that can be used in various fields.

Acknowledgement
This research was not funded by any grant.

References

[1] Chen, Z. Q., P. Cheng, and C. T. Hsu. "A theoretical and experimental study on stagnant thermal conductivity of bi-dispersed porous media." *International Communications in Heat and Mass Transfer* 27, no. 5 (2000): 601-610. https://doi.org/10.1016/S0735-1933(00)00142-1

[2] Vajravelu, K., K. V. Prasad, A. Sujatha, and Chiu-on Ng. "MHD flow and mass transfer of chemically reactive upper convected Maxwell fluid past porous surface." *Applied Mathematics and Mechanics* 33, no. 7 (2012): 899-910. https://doi.org/10.1007/s10483-012-1593-8

[3] Bég, O. Anwar, and Oluwole D. Makinde. "Viscoelastic flow and species transfer in a Darcian high-permeability channel." *Journal of Petroleum Science and Engineering* 76, no. 3-4 (2011): 93-99. https://doi.org/10.1016/j.petrol.2011.01.008

[4] Ziabakhsh, Z., and G. Domairry. "Solution of the laminar viscous flow in a semi-porous channel in the presence of a uniform magnetic field by using the homotopy analysis method." *Communications in Nonlinear Science and Numerical Simulation* 14, no. 4 (2009): 1284-1294. https://doi.org/10.1016/j.cnsns.2007.12.011

[5] Raftari, Behrouz, and Ahmet Yildirim. "The application of homotopy perturbation method for MHD flows of UCM fluids above porous stretching sheets." *Computers & Mathematics with Applications* 59, no. 10 (2010): 3328-3337. https://doi.org/10.1016/j.camwa.2010.03.018

[6] Sheikholeslami, M., M. Hatami, and D. D. Ganji. "Analytical investigation of MHD nanofluid flow in a semi-porous channel." *Powder Technology* 246 (2013): 327-336. https://doi.org/10.1016/j.powtec.2013.05.030

[7] Hassan, A. R., and O. J. Fenuga. "Flow of a Maxwell fluid through a porous medium induced by a constantly accelerating plate." *Journal of the Nigerian association of Mathematical Physics* 19 (2011).

[8] Jha, Basant Kumar. "Free-convection flow through an annular porous medium." *Heat and mass transfer* 41, no. 8 (2005): 675-679. https://doi.org/10.1007/s00231-003-0469-1

[9] Makinde, O. D. "Thermal ignition in a reactive viscous flow through a channel filled with a porous medium." (2006): 601-604. https://doi.org/10.1115/1.2188511

[10] Brown, G. O. "Henry Darcy and the making of a law." *Water Resources Research* 38, no. 7 (2002): 11-1. https://doi.org/10.1029/2001WR000727

[11] Fand, R. M., T. E. Steinberger, and P. Cheng. "Natural convection heat transfer from a horizontal cylinder embedded in a porous

[12] Sobamowo, M. G., A. T. Akinshilo, and A. A. Yinusa. "Thermo-magneto-solutal squeezing flow of nanofluid between two parallel disks embedded in a porous medium: effects of nanoparticle geometry, slip and temperature jump conditions." *Modelling and Simulation in Engineering* 2018 (2018). https://doi.org/10.1155/2018/7364634

[13] Russell, Alexander JB. "75th Anniversary of 'Existence of Electromagnetic–Hydrodynamic Waves'." *Solar Physics* 293, no. 5 (2018): 83. https://doi.org/10.1007/s11207-018-1296-3

[14] Selimefendigil, Fatih, and Hakan F. Öztop. "Corrugated conductive partition effects on MHD free convection of CNT-water nanofluid in a cavity." *International Journal of Heat and Mass Transfer* 129 (2019): 265-277. https://doi.org/10.1016/j.ijheatmasstransfer.2018.09.101

[15] Selimefendigil, Fatih, and Hakan F. Öztop. "Modeling and optimization of MHD mixed convection in a lid-driven trapezoidal cavity filled with alumina–water nanofluid: effects of electrical conductivity models." *International Journal of Mechanical Sciences* 136 (2018): 264-278. https://doi.org/10.1016/j.ijmecsci.2017.12.035

[16] Selimefendigil, Fatih, and Hakan F. Öztop. "Mixed convection of nanofluid filled cavity with oscillating lid under the influence of an inclined magnetic field." *Jou*

[17] Selimefendigil, Fatih, and Hakan F. Öztop. "Magnetic field effects on the forced convection of CuO-water nanofluid flow in a channel with circular cylinders and thermal predictions using ANFIS." *International Journal of Mechanical Sciences* 146 (2018): 9-24. https://doi.org/10.1016/j.ijmecsci.2018.07.011

[18] Selimefendigil, Fatih, Seda Özcan Çoban, and Hakan F. Öztop. "Electrical conductivity effect on MHD mixed convection of nanofluid flow over a backward-facing step." *Journal of Central South University* 5, no. 26 (2019): 1133-1145. https://doi.org/10.1007/s11771-019-4076-9

[19] Selimefendigil, Fatih, and Hakan F. Öztop. "Fluid-solid interaction of elastic-step type corrugation effects on the mixed convection of nanofluid in a vented cavity with magnetic field." *International Journal of Mechanical Sciences* 152 (2019): 185-197. https://doi.org/10.1016/j.ijmecsci.2018.12.044

[20] Raftari, Behrouz, and Kuppalapalle Vajravelu. "Homotopy analysis method for MHD viscoelastic fluid flow and heat transfer in a channel with a stretching wall." *Communications in nonlinear science and numerical simulation* 17, no. 11 (2012): 4149-4162. https://doi.org/10.1016/j.cnsns.2012.01.032

[21] Hatami, M., R. Nouri, and D. D. Ganji. "Forced convection analysis for MHD Al2O3–water nanofluid flow over a horizontal plate." *Journal of Molecular Liquids* 187 (2013): 294-301. https://doi.org/10.1016/j.molliq.2013.08.008

[22] Hatami, Mohammad, Mohsen Sheikholeslami, M. Hosseini, and Davood Domiri Ganji. "Analytical investigation of MHD nanofluid flow in non-parallel walls." *Journal of Molecular Liquids* 194 (2014): 251-259. https://doi.org/10.1016/j.molliq.2014.03.002

[23] Sheikholeslami, M., M. Gorji-Bandpy, and D. D. Ganji. "Numerical investigation of MHD effects on Al2O3–water nanofluid flow and heat transfer in a semi-annulus enclosure using LBM." *Energy* 60 (2013): 501-510. https://doi.org/10.1016/j.energy.2013.07.070

[24] Jasim, Abeer Majeed. "Exploration of No-Slip and Slip of Unsteady Squeezing Flow Fluid Through a Derivatives Series Algorithm." *Journal of Advanced Research in Fluid Mechanics and Thermal Sciences* 100, no. 1 (2022): 11-29. https://doi.org/10.37934/arfmts.100.1.1129

[25] Khan, Ansab Azam, Khairy Zaimi, Suliadi Firdaus Sufahani, and Mohammad Ferdows. "MHD flow and heat transfer of double stratified micropolar fluid over a vertical permeable shrinking/stretching sheet with chemical reaction and heat source." *Journal of Advanced Research in Applied Sciences and Engineering Technology* 21, no. 1 (2020): 1-14. https://doi.org/10.37934/araset.21.1.114

[26] Jasim, Abeer Majeed. "Study of the Impact of Unsteady Squeezing Magnetohydrodynamics Copper-Water with Injection-Suction on Nanofluid Flow Between Two Parallel Plates in Porous Medium." *Iraqi Journal of Science* (2022): 3909-3924. https://doi.org/10.24996/ijs.2022.63.9.23

[27] Hussein, Ahmed Kadhim, and Ahmed Waheed Mustafa. "Natural convection in fully open parallelogrammic cavity filled with Cu–water nanofluid and heated locally from its bottom wall." *Thermal Science and Engineering Progress* 1 (2017): 66-77. https://doi.org/10.1016/j.tsep.2017.03.002

[28] Besthapu, Prabhakar, Rizwan Ul Haq, Shankar Bandari, and Qasem M. Al-Mdallal. "Thermal radiation and slip effects on MHD stagnation point flow of non-Newtonian nanofluid over a convective stretching surface." *Neural Computing and Applications* 31 (2019): 207-217. https://doi.org/10.1007/s00521-017-2992-x

[29] Qasim, Muhammad, Zafar Hayat Khan, Ilyas Khan, and Qasem M. Al-Mdallal. "Analysis of entropy generation in flow of methanol-based nanofluid in a sinusoidal wavy channel." *Entropy* 19, no. 10 (2017): 490. https://doi.org/10.3390/e19100490

[30] Ganesh, N. Vishnu, Qasem M. Al-Mdallal, and Ali J. Chamkha. "A numerical investigation of Newtonian fluid flow with buoyancy, thermal slip of order two and entropy generation." *Case Studies in Thermal Engineering* 13 (2019): 100376. https://doi.org/10.1016/j.csite.2018.100376

[31] Aman, Sidra, Qasem Al-Mdallal, and Ilyas Khan. "Heat transfer and second order slip effect on MHD flow of fractional Maxwell fluid in a porous medium." *Journal of King Saud University-Science* 32, no. 1 (2020): 450-458. https://doi.org/10.1016/j.jksus.2018.07.007

[32] Ganesh, N. Vishnu, P. K. Kameswaran, Qasem M. Al-Mdallal, A. K. Hakeem, and B. Ganga. "Non-Linear thermal radiative marangoni boundary layer flow of gamma Al2O3 nanofluids past a stretching sheet." *Journal of Nanofluids* 7, no. 5 (2018): 944-950. https://doi.org/10.1166/jon.2018.1510

[33] Ramachandran, P. Subhadra, M. N. Mathur, and S. K. Ojha. "Heat transfer in boundary layer flow of a micropolar fluid past a curved surface with suction and injection." *International journal of Engineering science* 17, no. 5 (1979): 625-639. https://doi.org/10.1016/0020-7225(79)90131-9

[34] Berman, Abraham S. "Laminar flow in channels with porous walls." *Journal of Applied physics* 24, no. 9 (1953): 1232-1235. https://doi.org/10.1063/1.1721476

[35] Domairry, G., and M. Fazeli. "Homotopy analysis method to determine the fin efficiency of convective straight fins with temperature-dependent thermal conductivity." *Communications in Nonlinear Science and Numerical Simulation* 14, no. 2 (2009): 489-499. https://doi.org/10.1016/j.cnsns.2007.09.007

[36] Coşkun, Safa Bozkurt, and Mehmet Tarık Atay. "Fin efficiency analysis of convective straight fins with temperature dependent thermal conductivity using variational iteration method." *Applied Thermal Engineering* 28, no. 17-18 (2008): 2345-2352. https://doi.org/10.1016/j.applthermaleng.2008.01.012

[37] Sohrab, Siavash H., H. C. Catrakis, and F. K. Benra. "Derivation of invariant forms of conservation equations from the invariant Boltzmann equation." *Theoretical and Experimental Aspects of Fluid Mechanics* (2008): 27-35.

[38] andGbeminiyi Sobamowo, George Oguntala. "Galerkin's method of weighted residual for a convective straight fin with temperature-dependent conductivity and internal heat generation." *International Journal of Engineering and Technology* 6, no. 12 (2016).

[39] Filobello-Nino, Uriel, Hector Vázquez-Leal, K. Boubaker, Y. Khan, A. Perez-Sesma, A. Sarmiento-Reyes, V. M. Jimenez-Fernandez *et al.,* "Perturbation method as a powerful tool to solve highly nonlinear problems: the case of Gelfand's equation." *Asian Journal of Mathematics & Statistics* 6, no. 2 (2013): 76. https://doi.org/10.3923/ajms.2013.76.82

[40] Lim, C. W., and B. S. Wu. "A modified Mickens procedure for certain nonlinear oscillators." *Journal of Sound and Vibration* 257, no. 1 (2002): 202. https://doi.org/10.1006/jsvi.2001.4233

[41] Cheung, Y. K., S. H. Chen, and SL1103708 Lau. "A modified Lindstedt-Poincaré method for certain strongly non-linear oscillators." *International Journal of Non-Linear Mechanics* 26, no. 3-4 (1991): 367-378. https://doi.org/10.1016/0020-7462(91)90066-3

[42] Lewis, Roland W., Perumal Nithiarasu, and Kankanhalli N. Seetharamu. *Fundamentals of the finite element method for heat and fluid flow*. John Wiley & Sons, 2004. https://doi.org/10.1002/0470014164

[43] Sobamowo, M. G., L. O. Jayesimi, and M. A. Waheed. "Magnetohydrodynamic squeezing flow analysis of nanofluid under the effect of slip boundary conditions using variation of parameter method." *Karbala International Journal of Modern Science* 4, no. 1 (2018): 107-118. https://doi.org/10.1016/j.kijoms.2017.12.001

[44] Kargar, A., and M. Akbarzade. "Analytic solution of natural convection flow of a non-newtonian fluid between two vertical flat plates using homotopy perturbation method (HPM)." *World Applied Sciences Journal* 20, no. 11 (2012): 1459-1465.

[45] Ganesh, N. Vishnu, Ali J. Chamkha, Qasem M. Al-Mdallal, and P. K. Kameswaran. "Magneto-Marangoni nano-boundary layer flow of water and ethylene glycol based γ Al2O3 nanofluids with non-linear thermal radiation effects." *Case Studies in Thermal Engineering* 12 (2018): 340-348. https://doi.org/10.1016/j.csite.2018.04.019

[46] Ganesh, N. Vishnu, Qasem M. Al-Mdallal, and P. K. Kameswaran. "Numerical study of MHD effective Prandtl number boundary layer flow of γ Al2O3 nanofluids past a melting surface." *Case Studies in Thermal Engineering* 13 (2019): 100413. https://doi.org/10.1016/j.csite.2019.100413

[47] Rehman, Khalil Ur, Qasem M. Al-Mdallal, and M. Y. Malik. "Symmetry analysis on thermally magnetized fluid flow regime with heat source/sink." *Case Studies in Thermal Engineering* 14 (2019): 100452. https://doi.org/10.1016/j.csite.2019.100452

[48] Joneidi, A. A., D. D. Ganji, and M. Babaelahi. "Micropolar flow in a porous channel with high mass transfer." *International Communications in Heat and Mass Transfer* 36, no. 10 (2009): 1082-1088. https://doi.org/10.1016/j.icheatmasstransfer.2009.06.021

[49] Pour, M. Saffari, and SA Gandjalikhan Nassab. "Numerical investigation of forced laminar convection flow of nanofluids over a backward facing step under bleeding condition." *Journal of Mechanics* 28, no. 2 (2012): N7-N12. https://doi.org/10.1017/jmech.2012.45

[50] Arslanturk, Cihat. "A decomposition method for fin efficiency of convective straight fins with temperature-dependent thermal conductivity." *International communications in heat and mass transfer* 32, no. 6 (2005): 831-841. https://doi.org/10.1016/j.icheatmasstransfer.2004.10.006

[51] Rashidifar, Mohammad Amin, and Ali Amin Rashidifar. "Analysis of vibration of a pipeline supported on elastic soil using differential transform method." *American Journal of Mechanical Engineering* 1, no. 4 (2013): 96-102. https://doi.org/10.12691/ajme-1-4-4

[52] Sobamowo, M. G., and A. T. Akinshilo. "Analysis of flow, heat transfer and entropy generation in a pipe conveying fourth grade fluid with temperature dependent viscosities and internal heat generation." *Journal of Molecular Liquids* 241 (2017): 188-198. https://doi.org/10.1016/j.molliq.2017.05.145

[53] Dogonchi, A. S., and D. D. Ganji. "Analytical solution and heat transfer of two-phase nanofluid flow between non-parallel walls considering Joule heating effect." *Powder Technology* 318 (2017): 390-400. https://doi.org/10.1016/j.powtec.2017.06.018

[54] Akinshilo, Akinbowale T., and Osamudiamen Olaye. "On the analysis of the Erying Powell model based fluid flow in a pipe with temperature dependent viscosity and internal heat generation." *Journal of King Saud University-Engineering Sciences* 31, no. 3 (2019): 271-279. https://doi.org/10.1016/j.jksues.2017.09.001

[55] Berezantsev, V. G., M. I. Gorbunov-Posadov, and M. V. Malyshev. "Soil mechanics." (1964): 333-336. https://doi.org/10.1007/BF01704074

[56] Mohamed, Kezzar, Sari Mohamed Rafik, B. O. U. R. E. N. A. N. E. Rabah, Mohammad Mehdi Rashidi, and H. A. I. A. H. E. M. Ammar. "Heat transfer in hydro-magnetic nano-fluid flow between non-parallel plates using DTM." *Journal of Applied and Computational Mechanics* 4, no. 4 (2018): 352-364.

[57] Khan, Hamid, Mubashir Qayyum, Omar Khan, and Murtaza Ali. "Unsteady squeezing flow of Casson fluid with magnetohydrodynamic effect and passing through porous medium." *Mathematical Problems in Engineering* 2016 (2016). https://doi.org/10.1155/2016/4293721

[58] Rahimi-Gorji, Mohammad, O. Pourmehran, Mofid Gorji-Bandpy, and D. D. Ganji. "Unsteady squeezing nanofluid simulation and investigation of its effect on important heat transfer parameters in presence of magnetic field." *Journal of the Taiwan Institute of Chemical Engineers* 67 (2016): 467-475. https://doi.org/10.1016/j.jtice.2016.08.001

[59] Rahimi-Gorji, Mohammad, O. Pourmehran, Mohammad Hatami, and D. D. Ganji. "Statistical optimization of microchannel heat sink (MCHS) geometry cooled by different nanofluids using RSM analysis." *The European Physical Journal Plus* 130 (2015): 1-21. https://doi.org/10.1140/epjp/i2015-15022-8

[60] Biglarian, M., M. Rahimi Gorji, O. Pourmehran, and G. Domairry. "H2O based different nanofluids with unsteady condition and an external magnetic field on permeable channel heat transfer." *International Journal of Hydrogen Energy* 42, no. 34 (2017): 22005-22014. https://doi.org/10.1016/j.ijhydene.2017.07.085

[61] Mosayebidorcheh, Sobhan, Mohammad Rahimi-Gorji, D. D. Ganji, Taha Moayebidorcheh, O. Pourmehran, and M. Biglarian. "Transient thermal behavior of radial fins of rectangular, triangular and hyperbolic profiles with temperature-dependent properties using DTM-FDM." *Journal of Central South University* 24 (2017): 675-682. https://doi.org/10.1007/s11771-017-3468-y

[62] Al-Saif, Abdul-Sattar, and Assma Harfash. "Perturbation-iteration algorithm for solving heat and mass transfer in the unsteady squeezing flow between parallel plates." *Journal of Applied and Computational Mechanics* 5, no. 4 (2019): 804-815.

[63] Jasim, Abeer M. "Analytical approximation of the first grade MHD squeezing fluid flow with slip boundary condition using a new iterative method." *Heat transfer* 50, no. 1 (2021): 733-753. https://doi.org/10.1002/htj.21901

[64] Jasim, Abeer Majeed. "New Analytical Study for Nanofluid between Two Non-Parallel Plane Walls (Jeffery-Hamel Flow)." *Journal of Applied and Computational Mechanics* 7, no. 1 (2021): 213-224.

[65] Fahmy, M., M. Morsy, H. Abd Elshakour, and A. M. Belal. "Effect of thermal insulation on building thermal comfort and energy consumption in Egypt." *Journal of Advanced Research in Applied Mechanics* 43, no. 1 (2018): 8-19.

[66] Sharafatmandjoor, Shervin. "Effect of Imposition of viscous and thermal forces on Dynamical Features of Swimming of a Microorganism in nanofluids." *Journal of Advanced Research in Micro and Nano Engineering* 8, no. 1 (2022): 1-8.

[67] Abidin, Nurul Hafizah Zainal, Nor Fadzillah Mohd Mokhtar, Izzati Khalidah Khalid, and Siti Nur Aisyah Azeman. "Oscillatory Mode of Darcy-Rayleigh Convection in a Viscoelastic Double Diffusive Binary Fluid Layer Saturated Anisotropic Porous Layer." *Journal of Advanced Research in Numerical Heat Transfer* 10, no. 1 (2022): 8-19.

[68] Teh, Yuan Ying, and Adnan Ashgar. "Three dimensional MHD hybrid nanofluid Flow with rotating stretching/shrinking sheet and Joule heating." *CFD Letters* 13, no. 8 (2021): 1-19. https://doi.org/10.37934/cfdl.13.8.119